Generation of Squeezed Light Via Second Harmonic Generation

by

Phillip Tsefung Nee

Submitted to the Department of Electrical Engineering and Computer Science
in partial fulfillment of the requirements for the degree of

Master of Science in Electrical Engineering and Computer Science

at the

MASSACHUSETTS INSTITUTE OF TECHNOLOGY

February 1994

Author .....
Department of Electrical Engineering and Computer Science
January 24, 1994

Certified by .....
Dr. Roy Bondurant
Leader, Optical Communications Technology Group, MIT Lincoln Laboratory
Thesis Supervisor

Accepted by .....
Frederick R. Morgenthaler
Chairman, Departmental Committee on Graduate Students

Generation of Squeezed Light Via Second Harmonic Generation

by

Phillip Tsefung Nee

Submitted to the Department of Electrical Engineering and Computer Science
on January 14, 1994, in partial fulfillment of the
requirements for the degree of
Master of Science in Electrical Engineering and Computer Science

Abstract

The purpose of this thesis is to assess the feasibility of using semiconductor lasers and a monolithic $KNbO_3$ cavity to generate squeezed states of light. An experimental setup designed to detect amplitude squeezing via second harmonic generation from a doubly resonant $KNbO_3$ monolithic cavity was constructed. Based on the experimentally determined cavity parameters, a critical power of 3.5mW and a critical frequency of 400MHz are predicted. The maximum achievable amount of amplitude squeezing at an input power equal to the predicted critical power is determined to be 31% at the fundamental and 79% at the second harmonic. Excess noise from the diode laser prevented observation of squeezing.

Thesis Supervisor: Dr. Roy Bondurant
Title: Leader, Optical Communications Technology Group, MIT Lincoln Laboratory

Acknowledgments

First and foremost, I would like to thank Roy Bondurant, my research advisor, for affording me the oppotunity to work on this project and for providing me with continued guidance throughout the course of the project. I'd also like to express my gratitude to my supervisor Jeff Livas, from whom I learned an inordinate amount of practical knowledge and skills from a variety of fields. Above all, I'd like to thank him for his guidance and support throughout the course of the project and for being a truly classy individual to work with. Then I'd like to express my heart-felt thanks to Josephine Cappiello for constructing and repairing a number of much-needed hardware for the experiment and for providing generous technical assistance whenever I needed it. Then there's Fred Walther, whom I'd like to thank for lending me a paraphernalia of instruments and devices such as the 100mW diode laser, the blue filter, and the one-pass $KNbO_3$ crystal. I'd like to thank Ron Sprague for making the mounts for the crystal and helping me with a variety of machining jobs. I'd like to thank Jean Mead for the various secretarial help such as scheduling talks and typing up memos. Among others to whom I'd like to say thanks are Eric Swanson, Laura Adams, David Cruciolli, Fred Beihold, and Al Tidd for their generosity in lending me a variety of tools, instruments, and devices.

Contents

Chapter 1

Introduction

Random fluctuations of electromagnetic fields, dictated by the uncertainty principle in quantum mechanics, set the ultimate limit on the amount of precision possible in transmitting information by photons, or light. It is anticipated that, in the near future, many communications sytems which use light to transmit information will progress to the point where the accuracy of the transmitted information is limited by the random fluctuations in the optical field. Is there a way to reduce such fluctuations? Squeezed light allows one to redistribute the noise in an optical field such that the noise in one component of the field is less than that for classical light while the noise in the other component exceeds that of classical light. This offers the potential for using only the squeezed part of the light to transmit the information, thus improving the precision beyond that for classical light.

1.1 Thesis Outline

This thesis describes an experimental setup aimed at generating squeezed light from a potassium niobate crystal via the nonlinear optical process of second harmonic generation. The thesis is organized into the following chapters. The rest of this chapter consists of three sections. Section 1.2 provides a qualitative description of squeezing. In particular, a distinction is drawn between quadrature and amplitude squeezing. Also, some potential applications of squeezed light are discussed. In section 1.3 the

various physical processes that produce squeezed light are described, followed by a discussion of past experimental results by others in the generation of squeezed light. Section 1.4 discusses the motivation and general features of this experiment. Chapter 2 provides an extensive treatment of squeezing via second harmonic generation inside a doubly resonant cavity. The experimental setup is described in Chapter 3. Chapters 4 through 9 outlines the general progress of the experiment. The results achieved in the experiment will also be discussed in these chapters. A summary of the experiment and the results will be included in Chapter 10 along with a few concluding remarks.

1.2 Squeezed States

1.2.1 Qualitative description

At a given point in space a monochromatic electromagnetic wave of frequency ω can be specified by its amplitude and phase or by its sine and cosine components:

$$E(t) = Acos(\omega t + \phi)$$

$$E(t) = acos\omega t + bsin\omega t \tag{1.1}$$

According to quantum theory, the two components A, ϕ or a, b that specify the field are noncommuting operators and are therefore subject to the constraints of Heisenberg's uncertainty principle. That is, the two components cannot be known with absolute certainty simultaneously. In fact the product of their uncertainties must always be equal to or larger than a fundamental constant proportional to Planck's constant h. It is possible, however, to manipulate the field in such a way that the uncertainty in one component is reduced at the expense of increasing the uncertainty in the other component while the product of their uncertainties remain unchanged. The component whose uncertainty is reduced is appropriately described as the "squeezed" component[28].

In classical light, such as light emitted by a coherent laser, the uncertainties in the

sine and cosine components of the field are equal, and the uncertainty in the amplitude of the field obeys a Poisson distribution. In quadrature-squeezed light the uncertainty in either the sine or cosine component is decreased while that in the other component is correspondingly increased. In amplitude-squeezed light, the uncertainty in the intensity number is reduced to below the shot noise limit characteristic of classical light at the expense of increasing the uncertainty in the phase of the field. It is also possible to generate phase-squeezed light, the direct counterpart to amplitude-squeezed light.

1.2.2 Applications of squeezed states of light

Amplitude-squeezed light finds potential use in communications systems or in measurements that require very high precision[28][22]. In optical communications systems, for example, the information to be transmitted can be encoded on the amplitude (squeezed) quadrature of light. A detection scheme that is sensitive to the amplitude but not to the phase of the transmitted light would then record the information and thus improve the signal-to-noise ratio beyond that for a shot-noise-limited system. Other applications of squeezed light involve areas such as gravitational wave detection and optical ring gyroscope, where squeezed light offers a potential improvement by increasing the sensitivity of the detection scheme.

1.3 Methods of Generating Squeezed Light

1.3.1 Possible Methods In General

Experimentally, squeezed states of light have been generated since 1985[30]. Both quadrature-squeezed and amplitude-squeezed light have been produced by a variety of experimental configurations. Up to the present squeezed light has been generated by various forms of three-wave or four-wave mixing nonlinear optical processes and also by diode laser outputs which are below shot-noise[31][14]. In a four-wave mixing process, as shown in Figure 1a, four lightwaves interact via a nonlinear medium. The

nonlinear medium is often in the form of a nonlinear crystal, but the medium can be gaseous or liquid as well. Two strong counterpropagating pump fields E_1, E_2 of angular frequencies ω_1, ω_2 and two other fields E_3, E_4 of frequencies ω_3, ω_4 interact in the nonlinear medium. The fields obey energy conservation $\omega_1 + \omega_2 = \omega_3 + \omega_4$ and momentum conservation $\bar{k}_1 + \bar{k}_2 = \bar{k}_3 + \bar{k}_4$. Assuming $\omega_1 = \omega_2 = \omega$, a weak input field E_3 of frequency ω will give rise to an output field E_4 whose frequency is $\omega_4 = \omega$ and whose complex amplitude is everywhere the complex conjugate of E_3. Adding the two fields E_3 and E_4 interferometrically results in a new field that is quadrature-squeezed.

The general class of nonlinear optical processes called three-wave mixing has also produced both quadrature- and amplitude-squeezed light. Some of the best results in squeezing were achieved with optical parametric oscillation. In optical parametric oscillation (Figure 1b) an input field of frequency ω_p interacts with a nonlinear medium to produce two output fields of frequencies ω_1 and ω_2 such that $\omega_p = \omega_1 + \omega_2$. In the so-called dengerate optical parametric oscillator, $\omega_1 = \omega_2 = \frac{1}{2}\omega_p$. Anticorrelation in the distribution of photons from the two output fields gives rise to quadrature- or amplitude-squeezing in the two output fields. The type of squeezing that is manifested depends on the specific detection scheme used.

Second harmonic generation, another three-wave mixing process, has also been employed to generate amplitude-squeezed light. In second harmonic generation (Figure 1c) an input field at frequency ω gives rise to a second field at frequency 2ω inside a nonlinear medium. The output consists of both the second harmonic field and a residual field at the fundamental frequency ω. The nonlinear interactions introduce anticorrelation in the distribution of photons in both the fundamental and the second harmonic output fields such that both fields are amplitude-squeezed. Second harmonic generation is the method used in this work for generating squeezed light. A more detailed discussion of amplitude-squeezeing via second harmonic generation follows in the next chapter.

1.3.2 Past Experimental Accomplishments By Others

The first experimental demonstration of squeezed light was achieved by R. Slusher et. al. in 1985[26]. In their setup quadrature-squeezed light was generated by non-degenerate four-wave mixing due to sodium atoms in an optical cavity. A balanced homodyne detection system was used to measure the quadrature components of the output beam from the cavity. It was found that the fluctuation of one of the two quadratures was below the vacuum noise level. A modest amount of noise reduction (7%) below shot noise level was observed. Several other groups also generated squeezed states around the same time, all involving four-wave mixing of some kind but showing only modest amounts of noise reduction[15][23][21].

The most spectacular results in squeezing to date involve the process of parametric downconversion as described in the previous section. Wu et. al. demonstrated a 60% reduction in quadrature noise below the shot noise level in 1987[29][30]. In their setup the output of a $Nd{:}YAG$ laser at a wavelength of $\lambda = 1062$nm was frequency doubled inside a $Ba_2NaNb_5O_{15}$ crystal to generate a second harmonic beam at $\lambda = 531$nm. This beam served as the pump field to the optical parametric oscillator. A lithium niobate crystal doped with magnesium oxide ($LiNbO_3{:}MgO$) was used as the nonlinear medium for parametric downconversion. The crystal was placed inside an external cavity to increase the efficiency of conversion. The quadrature-squeezed signal field was then detected by balanced homodyne detection.

In 1989 T. Debuisschert et. al. reported a setup that exploits the anticorrelation in photon distribution between the signal and idler outputs generated by a non-degenerate optical parametric oscillator[4]. A noise reduction of 69% was observed in the difference in the intensities of the signal and idler outputs. Amplitude squeezing was generated in this case, since the noise reduction involves the relative intensities of the two outputs. The pump field was driven by an argon ion laser at a wavelength of $\lambda = 528$nm. The optical parametric oscillator consists of a KTP crystal placed inside an external cavity. The wavelengths of the signal and idler fields were at $\lambda_s = 1048$nm and $\lambda_i = 1067$nm, respectively. The two output fields were separated by a polarizer and detected by separate photodetectors. Intensity noise reduction below the shot

noise level in the difference between the two photodetector outputs was then observed on a spectrum analyzer. Other published results in squeezing using the parametric downconversion process are given in the bibliography[25][7][27][16][17].

Squeezing via second harmonic generation was first reported by S. Periera et. al. in 1988[18]. Their setup consists of a $LiNbO_3$:MgO crystal placed inside an external cavity and pumped by a Nd:YAG laser at a wavelength of $\lambda = 1062$nm. A second harmonic output beam at a wavelength of $\lambda = 531$nm was generated. The reflected fundamental field was detected, and a 13 % reduction in the intensity fluctuation below the shot noise level was observed.

More recently, in 1992, Kurtz et. al. reported a 40% reduction in the intensity fluctuation of the second harmonic mode below the shot noise level[24][11]. In their setup a monolithic $LiNbO_3$:MgO cavity was used as the medium for second harmonic generation. The pump field at $\lambda = 1062$nm was generated by a Nd:YAG laser. The ends of the crystal were coated to resonate strongly at both the fundamental and the second harmonic wavelengths. The transmitted second harmonic output field was detected by balanced homodyne detection.

In the aforementioned setups involving squeezing via second harmonic generation, the nature of the squeezing generated is amplitude squeezing, since the second harmonic generation process introduces anticorrelation in the photon number distribution at both the fundamental and second harmonic wavelengths.

1.4 Motivation and general features for this work

As mentioned previously, this work involves the generation of amplitude-squeezed light via second harmonic generation inside a doubly resonant cavity. In this particular setup a monolithic cavity made up of potassium niobate ($KNbO_3$) serves as the nonlinear medium for second harmonic generation. The pump field is produced by a diode laser operating at a wavelength of $\lambda = 860$nm. The monolithic cavity is designed such that significant amplitude squeezing is expected at both the fundamental and the second harmonic wavelengths.

The primary motivation for this work is to design a setup that allows one to produce a compact, efficient, and relatively inexpensive source of squeezed light that may ultimately find use in optical communication systems. The diode laser's size and cost, compared to those of other laser systems, make it the natural candidate for such purposes. The use of $KNbO_3$ as the nonlinear medium provides two additional advantages. First, the limited output power of the diode laser makes it imperative that a material with a high optical nonlinearity be used. $KNbO_3$ possesses a strong nonlinear optical coefficient that significantly exceeds that of most other commonly used nonlinear materials such as $LiNbO_3$:MgO and KTP. As discussed in the previous chapter, there is an optimum power level (the critical power) at which the largest amount of squeezing can be generated. For $KNbO_3$ the critical power level is quite low, on the order of a few milliwatts. Of course, the critical power is also a sensitive function of the cavity loss rates at the fundamental and at the second harmonic wavelengths. Second, the phasematching temperature for $KNbO_3$ at a wavelength of $\lambda = 860$nm is around room temperature. Consequently, there is no need to heat the crystal to high temperatures, as is the case for systems involving $LiNbO_3$, where the phasematching temperature at $\lambda = 1062$nm is about 123°C. The phasematching consideration is also the main reason for selecting $\lambda = 860$nm as the wavelength for the pump field.

Table 1 provides a summary of the general features of past accomplishments in squeezing via second harmonic generation and of the work described by this thesis.

Table 1. Experiments Involving Squeezing Via Second Harmonic Generation

Features	Pereiva et. al. (1988)	Kurz et. al. (1992)	This work
Material	$LiNbO_3$:MgO	$LiNbO_3$:MgO	$KNbO_3$
Cavity design	external	monolithic	monolithic
Type of laser	Nd:YAG	Nd:YAG	diode
Wavelength	1062nm	1062nm	860nm
Phasematching temperature	123°C	123°C	27°C
Critical power	1.6W	200mW	3.5mW
Observed squeezing	13%	40%	—

Chapter 2

Generation of Squeezed States Via SHG Inside a Doubly Resonant Cavity

The observation of second harmonic generation in the early 1960's marked the birth of nonlinear optics. Second harmonic generation is the most fundamental and best understood optical nonlinear interaction. In this chapter the basic theory of second harmonic generation and a number of practical issues in nonlinear optics such as phasematching and the use of a resonator to generate second harmonic generation are discussed.

2.1 Mathematical Description of Second Harmonic Generation

In a nonlinear medium the electric field of the incident radiation induces a nonlinear polarization whose magnitude and phase are given by the product of the incident fields. The expression for the nonlinear polarization is given as follows[31, p. 384]:

$$P_i = \epsilon_o \chi_{ij} E_j + 2\epsilon_o d_{ijk} E_j E_k + 4\epsilon_o d_{ijkl} E_j E_k E_l + ... \tag{2.1}$$

where χ_{ij} is the linear susceptibility tensor, and d_{ijk}, d_{ijkl} ..... are the optical nonlinearity tensors that relates the induced nonlinear polarization to the products of the incident fields. In the special case of second harmonic generation, the relevant nonlinear polarization is

$$P_i(\omega_2) = \epsilon_o d_{ijk} E_j(\omega_1) E_k(\omega_1) \tag{2.2}$$

where $\omega_2 = 2\omega_1$[5]. The subscript i refers to the cartesian components of the polarization vector.

From Maxwell's equations with the constitutive relation

$$\bar{D} = \epsilon_o \bar{E} + \bar{P}_{linear} + \bar{P}_{nonlinear} \tag{2.3}$$

one obtains the wave equation

$$(\nabla^2 - \mu_o \sigma \frac{\partial}{\partial t} - \mu_o \epsilon \frac{\partial^2}{\partial t^2}) \bar{E}(2\omega) = \mu_o \frac{\partial^2}{\partial t^2} \bar{P}_{NL}(2\omega) \tag{2.4}$$

Mathematically the nonlinear polarization serves as the source term in the wave equation for the second harmonic field. Assuming the fields propagate in the z-direction and ignoring propagation losses, the steady state second harmonic field amplitude is related to the fundamental field amplitude by

$$\frac{\partial}{\partial z} \mathcal{E}(2\omega) = -j \frac{\omega \mu_o c}{2n} \epsilon_o d_{eff} \mathcal{E}(\omega) \mathcal{E}(\omega) exp[j(k - k_p)z] \tag{2.5}$$

where $k_p = 2k(\omega)$, $k = k(2\omega)$, and d_{eff} is the effective nonlinear coefficient. Note also that the field amplitude $\mathcal{E}$ is related to the total field E by

$$E(z,t) = \mathcal{E}(z) exp(jkz - \omega t) \tag{2.6}$$

2.2 Phasematching

Integrating (2.5) one can determine the second harmonic field amplitude as a function of distance. The conversion efficiency to the second harmonic is optimized when the two fields are phasedmatched. That is, when $k(2\omega) = 2k(\omega)$ or $n(2\omega) = 2n(\omega)$, where n, the refractive index, is related to k by $k = \frac{2\pi n}{\lambda}$, λ being the wavelength. Physically, phasematching describes the condition at which the phase velocities of the fundamental and the second harmonic fields are identical. For most commonly used nonlinear materials, the index of refraction can be tuned by a number of parameters: frequency (wavelength), temperature, orientation of the crystal axes with respect to the incident wave, and electric field. In this work, the indices of refraction at the fundamental and the second harmonic wavelengths are adjusted by temperature and by an applied field across the nonlinear medium. The orientation of the crystal axes with respect to the incident wave is fixed.

In normally dispersive materials the index of refraction decreases with the wavelength of the field[31, p. 394]. In anisotropic materials two independent propagation modes exist, each with a different index of refraction[31, p. 87]. The two modes correspond to two orthogonally polarized electric displacement vectors $\bar{D}$. The direction of propagation specified by the $\bar{k}$ vector is normal to the plane formed by the two allowed $\bar{D}$ vectors. Figure 2 shows how phasematching is possible. Provided that the fundamental and second harmonic fields are polarized orthogonally to each other and thus corresopond to the two independent popagation modes, phasematching is achieved when the index of one mode at the fundamental wavelength is matched to the index of the other mode at the second harmonic wavelength. The tuning curve of one of the modes, the so-called extraordinary mode, is a function of the orientation of the crystal axes with respect to the incident wave[31, p. 92]. While the orientation is fixed in this experiment because of the use of a monolithic cavity, it is a tuning parameter for phasematching in many other applications. Figure 3 shows the nonlinear $KNbO_3$ crystal employed in this experiment and its corresponding crystal axes. The crystal is biaxial with principal indices of refraction $n_c < n_a < n_b$[1]. The indices of

refraction of the two propagation modes can be determined from the principal indices of refraction using the index ellipsoid method[31, p. 90]. The incident light propagates along the a-axis and is polarized along the b-axis. The transmitted second harmonic field is polarized along the c-axis, while the transmitted fundamental field remains polarized along the b-axis. The two independent modes of propagation correspond to the b-polarized fundamental wave and the c-polarized second harmonic wave with indices of refraction n_b and n_c, respectively.

2.2.1 Phasematching by temperature

To satisfy the phasematching condition the condition $n_b(\omega) = n_c(2\omega)$ must be satisfied. In general, both indices of refraction are functions of temperature. That is, $n_b(\omega) = n_b(\omega, T)$ and $n_c(\omega) = n_c(\omega, T)$. Shown in Figure 4 is the dependence of the indices of refraction as a function of temperature for $KNbO_3$ at a wavelength $\lambda = 860$ nm (or $\omega = 2.19 \times 10^{15}/s$). It is clear from the figure the phasematching condition is satisfied around 27^o C. It should be emphasized that Figure 4 is valid only at a wavelength of $\lambda = 860$nm. The phasematching temperature of $KNbO_3$ is a sensitive function of wavelength, as shown in Figure 5.

2.2.2 Phasematching by electro-optic effect

The index of refraction of a nonlinear material can also be tuned by applying a dc electric field. This effect is called the electro-optic effect. The change in the index of refraction is related to the applied field by the following equation[31]:

$$\Delta \left(\frac{1}{n^2}\right)_{ij} = \sum_k \frac{1}{2} n^3 r_{ijk} E_k \tag{2.7}$$

Here r_{ijk} is the (third-ranked) electro-optic tensor, and the cartesian coordinate system is that of the crystal axes of the nonlinear material. The indicies of refraction are given as tensor elements in the above equation. To find the change in index of refraction along a given direction, one must diagonalize the 3×3 tensor and determine the new set of principal axes, which is generally different from the crystal axes of the

nonlinear material. Assoicated with each principal axis is a new index that may be a function of the applied electric field. The projection of the direction of interest on the principal axes allows one to determine the index for a field polarized along that direction. For an electric field applied across the c-axis as shown, the electro-optic tensors that contribute to the index change are r_{113}, r_{123}, r_{133}, r_{223}, r_{233} and r_{333}. In the case of $KNbO_3$, all of the above tensor elements are identically zero except for r_{333}. Therefore, the change in index is entirely along the c-axis, implying that $n_c(2\omega)$ can be adjusted independently of $n_b(\omega)$ by the applied field. This is not the case for temperature tuning, where both $n_c(2\omega)$ and $n_b(\omega)$ vary with temperature.

2.3 SHG Inside A Doubly Resonant Cavity

In general the efficiency of second harmonic generation from a single pass crystal is rather limited. One way to improve the efficiency of second harmonic generation is to place the nonlinear crystal inside an optical resonator. In a resonator, light essentially makes many passes through the nonlinear crystal before leaving the resonator, thereby effectively increasing the interaction length. Furthermore, "mirrors" can be directly deposited on the end facets of the crystal to form a resonator, such that physically the crystal and the cavity are identical. Such "mirrors" are usually realized by depositing a dielectric that is highly reflecting at the wavelength(s) of interest onto the crystal. This type of cavity is commonly referred to as a monolithic cavity. In this experiment a $KNbO_3$ monolithic cavity that is resonant at both the fundamental and the second harmonic wavelengths is employed. The rest of the section will be devoted to a discussion of second harmonic generation inside a doubly resonant cavity.

2.3.1 Achieving double-resonance and phasematching

At double-resonance the roundtrip phase of the fundamental and second harmonic fields must each be integer multiples of 2π:

$$\Phi_1 = k(\omega)l = \frac{2\pi n_b{}^{\omega}}{\lambda} l = 2\pi N$$

$$\Phi_2 = k(2\omega)l = \frac{2\pi {n_c}^{2\omega}}{\lambda} l = 2\pi M \tag{2.8}$$

Here N, M are integers, and l is the length of the crystal. ${n_c}^{2\omega}$ and ${n_b}^{\omega}$ are indices of refraction of the second harmonic field polarized along the c- and b-axis, respectively. To satisfy the double-resonance and phase-matching conditions simultaneously, one sets

$$\frac{{n_b}^{\omega}}{{n_c}^{2\omega}} = \frac{N}{2M} = 1$$

By definition the two refractive indices are equal under phasematched condition. However, phasematching is a sufficient but not a necessary condition for double resonance, provided that the physical cavity length is identical for the two fields. Double resonance can be achieved without phasematching (i.e. $N \neq 2M$), the penalty being reduced conversion efficiency to the second harmonic compared to the phasematched case.

2.3.2 Equations of motion

The semi-classical equations of motion describing second harmonic generation inside a Fabry-Perot resonator are[5]:

$$\frac{d}{dt}\alpha_1 = j\,\triangle_1\,\alpha_1 - \gamma_1\alpha_1 + \kappa\alpha_1^*\alpha_2 + \epsilon_1$$

$$\frac{d}{dt}\alpha_2 = j\,\triangle_2\,\alpha_2 - \gamma_2\alpha_2 - \frac{1}{2}\kappa\alpha_1^2 \tag{2.9}$$

where $*$ denotes the complex conjugate. Here normalized electric field amplitudes α_1, α_2, corresponding to the fundamental and second harmonic modes, respectively, are used. ϵ_1 is the pump amplitude at the fundamental frequency. γ_1 and γ_2 are the cavity loss rates for the two modes, and $\triangle_1$, $\triangle_2$ are frequency detunings from the resonant frequencies of the two modes. The parameter κ is the coupling coefficient between the two fields. It determines the amount of energy transfer between the two fields. Experimental determination of γ_1, γ_2, and κ is treated in Chapters 5 and 9.

The normalized field amplitudes are related to the actual field amplitudes by

$$\mathcal{E} = j\sqrt{\frac{2h\nu}{\epsilon_o V}}\alpha \tag{2.10}$$

where V is the mode volume, and $h\nu$ is the energy of a single photon of frequency ν. The equations of motion can be linearized around the steady state fields inside the cavity. In obtaining the steady state, one sets $\frac{d}{dt}\alpha_1 = 0$ and $\frac{d}{dt}\alpha_2 = 0$ and solves for the α_1 and α_2. The second harmonic amplitude can be shown to be a single-valued function of the normalized driving field ϵ_1:

$$2\gamma_2|\kappa\alpha_2|^3 + 4\gamma_1\gamma_2|\kappa\alpha_2|^2 + 2{\gamma_1}^2\gamma_2|\kappa\alpha_2| = |\kappa\epsilon_1|^2 \tag{2.11}$$

Here we have assumed zero detunings for simplicity. By carrying out an eigenvalue analysis of the equations of motion around the steady state operating point, one can show that the second harmonic mode becomes unstable and exhibits self-pulsing instability above a critical pump field[5]

$$\epsilon_{1c} = \frac{2\gamma_1 + \gamma_2}{\kappa}\sqrt{2\gamma_2(\gamma_1 + \gamma_2)} \tag{2.12}$$

The angular frequency at which this instability takes place is

$$\Omega_{crit} = \sqrt{\gamma_2(\gamma_1 + \gamma_2)} \tag{2.13}$$

The normalized quantity ϵ_1 is related to the actual power (in units of Watts) by the following expression:

$$P_{in} = \frac{\hbar\omega_1 \triangle t|\epsilon_1|^2}{1 - R_{in}} \tag{2.14}$$

where $\triangle t = \frac{2nl}{c}$ is the cavity roundtrip time; R_{in} is the power reflectivity of the input facet at $\lambda = 860$nm; n is the index at $\lambda = 860$nm; and l is the cavity length. This critical pump power is a key piece of information in the analysis of amplitude squeezing as described in the following section.

2.4 Amplitude squeezing via SHG

In the quantum mechanical description, second harmonic generation involves the simultaneous creation of one second harmonic photon and the annihilation of two photons from the fundamental mode. The incident driving field has Poissonian photon statistics. That is, the arrival rate of photons is perfectly random, exhibiting a Poissonian distriution:

$$P_n = \frac{< n >^n exp[- < n >]}{n!} \tag{2.15}$$

where $< n >$ is the average photon number detected in a given detection time interval. The second harmonic process converts photon-pairs in the fundamental mode to second harmonic photons. The photocounting distribution of the photon-pairs is sub-Poissonian, where its field fluctuation is less than that of the fundamental driving field. The photocounting distribution of second harmonic photons is related to that of the incident fundamental photons by

$$P_n(2\omega) = P_{2n}(\omega) + P_{2n+1}(\omega) \tag{2.16}$$

since for a given detection interval n second harmonic photons can be detected given $2n$ or $2n + 1$ fundamental photons in the same time interval. The intensity noise can be expressed as the mean square deviation from the average number of detected photons in a given detection interval. That is, $\triangle n = \sqrt{n^2 - < n >^2}$. For a Poissonian distribution the uncertainty in the number of photons is equal to the average number of photons:

$$\triangle n =< n >$$

Straightforward algebraic manipulation shows that the uncertainty in the photocounting distribution of the second harmonic photons is less than that for a Poissonian distribution. That is,

$$\triangle n(2\omega) \leq < n(\omega) >$$

Therefore, the second harmonic field exhibits sub-Poissonian photon statistics.

The photon statistics of the output fundamental field are also sub-Poissonian. One can view the second harmonic process as a process that selectively converts photons that are spaced closely together in a given detection interval. The second harmonic process thus removes bunched photons from the fundamental beam. This results in a more evenly spaced distribution of photons, implying reduced fluctuation in the average number of photons. By this argument the photon distribution is expected to be sub-Poissonian for the output fundamental field as well.

Mathematically, from the linearized equations of motion for a doubly resonant cavity discussed previously, the intensity fluctuation spectrum (in W/m^2) of the fundamental and second harmonic fields can be expressed as a function of the frequency Ω at which the spectrum is observed[10]:

$$\sqrt{< \mid \triangle I_1(\Omega)\mid^2 >} =< I_1 > (1 - \gamma_1 \mid \kappa\alpha_2 \mid \frac{{\gamma_2}^2 + \Omega^2}{D^2})$$

$$\sqrt{< \mid \triangle I_2(\Omega)\mid^2 >} =< I_2 > (1 - \gamma_2 \mid \kappa\alpha_2 \mid \frac{\mid \kappa\alpha_1 \mid^2}{D^2}) \qquad (2.17)$$

where

$$D^2 = [\mid \kappa\alpha_1 \mid^2 + \gamma_2(\gamma_1 + \mid \kappa\alpha_2 \mid) - \Omega^2]^2 + (\gamma_1 + \gamma_2 + \mid \kappa\alpha_2 \mid)^2\Omega^2$$

Here $< I_1 >$, $< I_2 >$ denote the average output intensities of the two modes. For frequencies much higher than the cavity loss rates γ_1, γ_2 the field fluctuations approach the shot-noise value characteristic of classical light. Since high measurements frquencies correspond to short observation time intervals, the amount of squeezing is degraded for observation time intervals shorter than the cavity lifetimes at the fundamental and the second harmonic because interactions between light and the cavity do not have time to occur. Shown in Figure 27a is a plot of the expected amplitude squeezing spectra as a function of measurement frequency for a set of experimentally determined parameters. Here V represents the noise powers of the fundamental and the second harmonic modes normalized to their shot noise values. At $V = 0$ perfect squeezing is obtained as the noise power approaches zero. It is clear that the choice of frequency at which the spectrum is observed depends on one's interest in observing

squeezing in the fundamental mode or in the second harmonic mode. The loss rates γ_1, γ_2 depend on the coated reflectivities of the two facets and absorbtion within the crystal, and the coupling coefficient κ is determined from the amount of depletion of the fundamental mode power by second harmonic generation. As expected, both the fundamental and second harmonic noise powers approach the shot noise level for frequencies larger than the cavity bandwidth.

Amplitude squeezing is also a function of the input power to the crystal. As mentioned in the previous section, the system exhibits self-sustained oscillations for $\epsilon \geq \epsilon_c$. The intensity fluctuation at the second harmonic wavelength decreases as ϵ is increased until the critical power ϵ_c is reached (Figure 28c). Hence, the critical pump power sets the power required for optimum amplitude squeezing.

A more complete discussion of the expected amount of amplitude squeezing as a function of measurement frequency and of input power to the crystal is provided in Chapter 9.

Chapter 3

Experimental Setup And Procedure

The complete experimental setup described by this thesis is shown in Figure 6. The diode laser output is driven by a constant current source and focused by a lens onto the monolithic cavity. Two Faraday isolators serve the purpose of preventing back reflections into the laser cavity. The incident beam is polarized vertically (normal to the page). After the incident beam passes through the polarizing beam splitter, the Faraday rotator rotates the polarization of the incident field by 45 degrees. The half-wave plate rotates the polarization of the incident field to the horizontal orientation, parallel to the b-axis of the $KNbO_3$ crystal. The transmitted fundamental and second harmonic outputs from the cavity are separated by a filter and detected by separate photodetectors. The reflected output from the cavity consists mainly of the fundamental field. Since the Faraday rotator is a non-reciprocal device, the reflected field, after passing back through the Faraday rotator, has orthogonal polarization with respect to the incident field. The polarizing beam splitter then steers the back-reflected field onto a photodetector. An rf synthesizer modulates the laser output. A set of locking electronics amplifies and demodulates the photodetector output to produce an error signal that feeds back to the laser bias current and thus stabilizes the frequency of the incident field. This frequency stabilization scheme for the fundamental field is commonly known as the Pound-Drever locking scheme and

will be discussed in more detail in Chapter 6[20].

A second set of locking electronics is used to stabilize the intensity of the second harmonic output to its peak. That is, to maintain phasematching between the fundamental and the second harmonic fields. The $KNbO_3$ crystal is temperature-controlled such that the two fields are in the vincinity of phasematching. A programmable high voltage supply produces a field which fine-tunes the phasematching via the electro-optic effect. An rf signal is superimposed on the dc field across the crystal, thereby modulating the intensity of the transmitted second harmonic output. A portion of the transmitted output is detected by a photodetector and then demodulated to give an error signal that progams the high voltage supply. Further discussion of this intensity stabilization scheme is provided in Chapter 6.

Chapter 4

Alignment of Crystal

4.1 Linear vs. Ring Resonator

The $KNbO_3$ crystal used in the experiment is configured as shown in Figure 7. The crystal can be used as either a ring resonator or a linear resonator as shown in the figure. The advantage of using the crystal in the ring configuration is that the reflected beam travels a different path from that of the incident beam. Therefore, no additional optics is necessary to separate the indident beam from the reflected beam. The drawback of using the ring cavity resonator is that the the fundamental and the second harmonic fields cannot be completely phasematched because the beam paths of the two fields do not overlap. This effect is illustrated in Figure 8. While it is possible to achieve phasematching between the fundamental and the second harmonic along the cavity axis using temperature and electro-optic tuning, the same is not true for the direction normal to the cavity axis (the b-axis). In the ring cavity design, parts of the beam path for the fundamental and the second harmonic have components along this transverse direction. Therefore, the two fields travel at different velocities inside the crystal even if they are phasematched in the longitudinal direction. Consequently, the two beams map out slightly different paths circulating the cavity.

Initially, the monolithic $KNbO_3$ crystal was set up as a ring cavity for the advantages mentioned previously. However, the problem of non-overlapping beams made it necessary to revert to the linear cavity set-up, which necessitates the addition of the

isolators to prevent feedback into the laser, of the polarizing beam splitter to steer the reflected beam into the photodetector, and of the polarizer and the half-wave plate to rotate the polarization of the reflected beam to 90 degrees relative to that of the incident beam.

4.2 Modematching

One major difficulty encountered in the experiment involves the modematching of the incident beam to the monolithic $KNbO_3$ cavity. The optimum beam waist inside a cavity depends on the geometry and size of the cavity as well as the laser wavelength. When modematched, the beam waist of the incident laser beam matches the optimum beam waist defined for the particular cavity in question. This normally involves using a carefully chosen focal lens to focus the incident beam to the desired beam waist inside the cavity. Failure to achieve modematching results in the presence of higher-order radial sidemodes as well as drastically reduced efficiency in the conversion to the second harmonic.

For an incoming gaussian beam of radius r focused by a lens of focal length f, the minimum spot size is[6, p. 141]

$$r_o = \frac{f\lambda}{\pi r} \tag{4.1}$$

where λ is the wavelength of the beam. The gaussian intensity profile of the optical beam assumed in (4.1) is, for all practical purposes, an adequate approximation of the diode laser output.

For a symmetrical optical cavity, the optimum beam waist for modematching is given by[31, p. 140]

$$r_o = \sqrt{\frac{\lambda}{n\pi}}[\frac{(2R-l)l}{4}]^{\frac{1}{4}} \tag{4.2}$$

Here R is the radius of curvature of the symmetric cavity; l is the physical length of the cavity; and n is the index of refraction of the cavity medium. For potassium niobate, $n = 2.28$. The $KNbO_3$ cavity employed in this experiement has a radius of curvature of 5cm and a cavity length of 7mm. The beam waist required for mode-

matching is determined to be 16.4μm. The incident laser beam has a beam radius of approximately 1mm. The beam is focused by a lens onto the monolithic cavity. The focal length necessary to achieve the desired beam waist of 16.4μm is calculated from (4.2) to be 6cm. In practice several lenses with different focal lengths were tried out one at a time. The lens with a focal length of 5cm gives the best conversion efficiency. Alignment of the cavity using focal lengths that give poor modematching is extremely difficult. Scanning the transmission spectrum reveals that the output intensity of the main mode is only slightly higher than that of the side modes under poor modematching. Under good modematching, the ratio between the main mode and side mode intensities is more than 10:1, although it is virtually impossible to completely extinguish the sidemodes.

Chapter 5

Determining Cavity Losses

The cavity loss rates γ_1, γ_2 are two of the key parameters used in determining the critical power for onset of self-pulsing oscillations and the amount of achievable amplitude squeezing. The cavity loss rates characterize the roundtrip loss of light inside the cavity due to transmission of power from the end mirrors and to absorbtion within the crystal. It is defined mathematically by the following equation:

$$\frac{d}{dt}E = -\gamma E \tag{5.1}$$

in the absence of any external driving term. Here E is the optical field inside the cavity.

5.1 Expression for Cavity Bandwidth

The cavity loss rates defined above is equivalent to the full-width-at-half-maximum bandwidth of the cavity transmission spectrum $\Delta\nu_{FWHM}$. Assuming that the power reflectivities of the cavity's input and output facets are R_1 and R_2, respectively, and that the length of the cavity is l,

$$\Delta\,\nu_{FWHM} = \frac{c}{2\pi n}(\alpha - \frac{1}{l}ln\sqrt{R_1R_2}) \tag{5.2}$$

under the approximations $\nu - \nu_o << c/2\pi nl$ and $\alpha l - ln\sqrt{R_1 R_2} << 1$. Here α is the distributed loss of optical power (with the unit cm^{-1}) due to absorbtion within the crystal, and n is the index of refraction of the nonlinear material. Specifically, the cavity loss rate γ and the cavity bandwidth are related by

$$\gamma = \pi \triangle \nu_{FWHM} \tag{5.3}$$

Appendix 1 provides a detailed outline of the derivations for γ and $\triangle\nu_{FWHM}$.

5.2 Measurement of Cavity Bandwidth—Fundamental Mode

In the fundamental mode, the cavity bandwidth is measured by scanning the frequency of the laser across at least one free spectral range, the frequency spacing between adjacent longitudinal cavity modes. The transmitted beam from the cavity is detected directly by a photodetector, and the transmitted intensity as a function of laser frequency is recorded on an oscilloscope. Figure 9 shows an oscilloscope trace of the transmitted intensity spectrum. From the oscilloscope trace the full-width-at-half-maximum bandwidth as a fraction of one free spectral range can be readily determined. The free spectral range is given in terms of the length of the cavity l and the index of refraction n by the relation

$$\nu_{FSR} = \frac{c}{2nl} \tag{5.4}$$

For the specific $KNbO_3$ cavity used in the experiment, the bandwidth was measured to be 201 ± 18 MHz, from which the cavity loss rate is calculated to be

$$\gamma_1 = (6.32 \pm .57) \times 10^8/s$$

5.3 Measurement of Cavity Bandwidth—Second Harmonic Mode

Determining the cavity bandwidth for the second harmonic mode is a more complicated problem experimentally. Whereas for the case of the fundamental mode the frequency of the laser can be tuned simply by adjusting the laser bias current, the same tachnique cannot be applied to the second harmonic case because the amount of conversion from fundamental to second harmonic is itself frequency dependent. A frequency tunable source of second harmonic output is required to probe the cavity at the second harmonic wavelength. Two methods have been attempted. In the first method the cavity is probed directly with a tunable blue laser source realized by sending the diode laser output beam through a single-pass $KNbO_3$ crystal to generate the second harmonic output. The frequency of the laser is then scanned across one free spectral range, and the transmitted spectrum is analyzed. However, with the available amount of input power from the laser, the amount of second harmonic power generated turns out to be insufficient because the detected intensity of the transmitted second harmonic beam is masked by the photodetector noise.

In the second method the index of refraction at the second harmonic wavelength is tuned instead of the laser frequency. The index tuning, which is achieved by varying the electric field applied across the crystal via the electro-optic effect, changes the effective cavity length at the second harmonic wavelength but not the at fundamental wavelength. The modulation of the effective cavity length implies a change in the resonance frequency of the cavity. The optical frequency of the fundamental and second harmonic fields are held fixed by feedback electronics. The two problems are complimentary of each other. In the case for the fundamental, the cavity length is fixed while the frequency of the optical field is varied. In the case for the second harmonic, the frequency of the optical field is held constant, but the cavity length is tuned. The voltage across the crystal is scanned across at least one free spectral range, and the transmitted signal is detected by a photodetector. The transmitted intensity as a function of the applied high voltage is recorded an the oscilloscope,

from which the full-width-at-half-maximum bandwidth can be measured directly. By measuring the change in the location of the transmission peak for a given amount of change in the applied voltage, one can convert the bandwidth to frequency units. Experimentally, the bandwidth at the second harmonic wavelength was measured to be 620 ± 15 MHz, which gives a cavity loss rate of

$$\gamma_2 = (1.95 \pm .05) \times 10^9/s$$

Chapter 6

Achieving Double Resonance Via Frequency Locking

As mentioned in Chapter 3, two sets of locking electronics are used to stabilize the frequency of the fundamental and second harmonic fields and the intensity of the second harmonic field, respectively. In this chapter the principles involved in the two locking schemes are discussed.

6.1 The Pound-Drever Locking Scheme

Shown in Figure 10 is a more detailed sketch of the setup for stabilizing the optical frequency of the laser output to one of the resonance frequencies of the monolithic cavity[2]. The frequency of the semiconductor diode laser is tuned by an injection current to the laser diode. The laser is modulated by superimposing an rf current signal to the injection current of the laser. In the frequency domain this modulation induces sidebands to the carrier frequency. The total field including the sidebands is given by[9]:

$$E \propto j \sum_{n=0,\infty} J_n(m) exp[j(\Omega + n\omega)t] + j \sum_{n=1,\infty} (-1)^n J_n(m) exp[j(\Omega - n\omega)t] + c.c. \quad (6.1)$$

where $J_n(m)$ are Bessel functions of integer order; m is the modulation index; and *c.c.* denotes the complex conjugate. The monolithic cavity in this case serves as a filter that transmits the carrier frequency but reflects the sidebands. This requires that the modulation frequency be roughly equal to or larger than the bandwidth of the cavity at the fundamental wavelength. The reflected field consists of the sidebands and some residual carrier.

Also shown in Figure 10 is the frequency spectrum of the field at various parts of the setup. The photodetector detects the beat signal between the carrier and the sidebands. The output of the photodetector can be decomposed into two components that are 90 degrees out of phase. One of the components is proportional to the difference between the magnitudes of the reflected sidebands. The other component is proportional to the difference between the phase of the carrier and the average of the phases of the sidebands. The magnitude of this phase difference is a sensitive function of the difference between the carrier frequency and the cavity resonance frequency. As shown in the figure, the phase difference $\triangle\phi$ has the properties of a discriminant curve. Namely, its sign changes at the origin, and the slope of the curve is maximized at the origin. The amplified photodetector output is then demodulated to baseband. The phase of the demodulating signal is adjusted such that the demodulated signal is proportional to the phase-sensitive component of the detector output. A loop filter is constructed to ensure stable operation of the feedback system. The output of the loop filter is summed with the bias current of the diode laser to adjust the frequency of the laser output. The loop filter circuit is shown in Figure 11. It consists of a gain stage followed by an integrator stage. The gain stage simply amplifies the demodulated signal to increase the slope of the discriminant curve mentioned above. The integrator stage provides the necessary compensation for stable operation of the overall feedback loop.

An oscilloscope trace of $\nu_o - \nu_c$ vs. the dc output signal is shown in Figure 12. How close the carrier frequency of the laser stays locked to the resonance frequency depends on the slope of this discriminator curve and also on the noise of the curve. The slope of the discriminator curve is a function of the modulation index which

measures the strength of modulation. For each modulation frequency there exists a modulation index which maximizes the slope of the discriminator curve[9]. However, it may not always be desirable to use such an optimum modulation index. As the moduation index is increased, power is transferred from the carrier to the sidebands, reducing the transmitted power from the cavity. At the modulation frequencies normally used in the experiment ($\approx$200MHz) the carrier power is severely attenuated as compared to the unmodulated case if modulated with the optimum modulation index. As a compromise, the laser is only weakly modulated in this experiment such that attenuation in the carrier power is low. A loop filter that follows amplifies the discriminator signal and provide the necessary compensation for loop stability. The price paid for by using electronic gain is that any noise associated with the discriminator curve will be amplified as well. In practice, this does not constitute a significant problem. Experimentally, the frequency of the laser was successfully stabilized to the cavity resonance for several hours without losing lock.

The treatment on the Pound-Drever locking scheme provided in this chapter is mostly qualitative. A more quantitative discussion can be found in Reference 2[2].

6.2 Locking the Second Harmonic Intensity

The setup for locking the intensity of the second harmonic to its maximum is shown in Figure 13. As mentioned in Chapter 2, the temperature of the crystal and the electro-optic voltage applied across the crystal are adjusted such that the crystal is in the vincinity of phasematching. An ac modulation signal at a frequency of 11.5MHz is summed with the high voltage bias. At a fixed temperature the intensity of the blue output is solely a function of the electro-optic voltage across the crystal. Therefore, the 11.5MHz signal in effect modulates the intensity of the second harmonic output.

A portion of the modulated second harmonic output intensity is detected by a photodetector, and the detected signal is then demodulated. As illustrated in Figure 13, the polarity of the demodulated output changes as the second harmonic intensity crosses its maximum value. A loop filter amplifies and compensates the demodulated

output before the signal is fed back to the programmable high voltage supply. The sign of the loop filter output is adjusted such that the sign of the feeback signal will always act to restore the intensity of the second harmonic field to its maximum.

Experimentally, the second harmonic output intensity was successfully stabilized to its maximum, producing a stable blue output beam, while the laser frequency remained locked to the cavity resonane. Uninterrupted "double-locking" was sustained for more than two hours.

6.3 Thermal Effect

6.3.1 Asymmetry in SH intensity as a function of temperature

A typical plot of the second harmonic output intensity as a function of temperature or electo-optic voltage is shown in Figure 14. The intensity distribution is symmetrical around its peak value. Experimentally it was found that such a symmetrical distribution is only true for low input powers, on the order of 1 mW or less. As the input power is increased, the intensity profile becomes increasingly asymmetrical, as shown in the dotted curve in Figure 14. Assuming the temperature of the crystal lies on the "flat" side of the curve initially, the intensity is gradually increased with decreasing temperature until the maximum (phasematched condition) is reached. However, as soon as the maximum is reached, the intensity drops precipitously even without any further decrease in temperature set by the temperature controller. To return to the phasematched condition again, the temperature needs to be increased by a certain amount before the intensity increases sharply to its peak again. Such a "hysteresis" curve is sketched in Figure 15. This behavior can be qualitatively explained by self-heating of the crystal. Along the path AB, the crystal is gradually cooled by the temperature controller as its second harmonic output intensity increases. As its output intensity increases, the crystal itself also generates some heat, even though its overall temperature continues to drop. Once the peak intensity is reached, the

continued cooling due to the temperature controller starts to decrease the output intensity. The self-heating of the crystal is thus reduced, causing the crystal to cool by itself. This cooling effect will act to further decrease the output intensity, which in turn cools the crystal even further. Such a positive feedback effect triggers a dramatic decrease in the output intensity (path BC), even if the temperature of the temperature controller remains constant once the peak output intensity is reached. If the temperature is now increased by adjusting the temperature controller, the crystal will gradually heat up again until its self-heating is sufficient to cause significant positive feedback, which results in a rapid increase in the output intensity (paths CD and DE). The "hysteresis" effect is a manifestation of the amount temperature change due to the crystal's self-heating.

6.3.2 Asymmetry in SH intensity as a function of electro-optic voltage

This asymmetry in second harmonic intensity exists for temperature tuning as well as for electro-optic voltage tuning. The qualitative behaviors are essentially the same for the two cases, even though the physical mechanisms by which the crystal is tuned are different. Currently there is no satisfactory explanation for this effect.

The steepness of the tuning curve on one side creates a slight problem for locking the second harmonic intensity. At low input powers the feedback electronics is capable of stabilizing the intensity to its maximum value. At high input powers, however, the gain of the locking loop is insufficient to hold the second harmonic output intensity from falling off the steep side of the tuning curve. Consequently, the intensity is stabilized to a point slightly on the flat side of the tuning curve. Experimentally, the second harmonic intensity could always be locked to within 10% of its true maximum.

Chapter 7

Noise Measurement and Analysis

One of the most important prerequisites to observing squeezed light is to ensure that the system is free of excess noise. The signature of amplitude squeezed light is the reduction of its intensity fluctuation below that of the shot noise level for classical light. It is therefore crucial that the noise detected by the detection scheme be dominated by the shot noise as opposed to other noise sources.

7.1 Shot Noise, Thermal Noise, RIN, and Amplifier Noise

The noise detection scheme for the reflected and the transmitted fields from the cavity is shown in Figure 16. Light is incident on a photodetector, generating a photocurrent. The photocurrent is then amplified by an ac-coupled rf amplifier. The output of the rf amplifier is then fed to a spectrum analyzer, from which the noise spectrum can be observed. The noise that is measured at the spectrum analyzer is dominated by four major noise sources, namely shot noise, thermal noise, relative intensity noise (RIN), and noise from the rf amplifiers.

The term "shot noise" used so far in this work refers to the Poissonian fluctuation in the photocurrent arising from the detection of classical light. This fluctuation is fundamental in nature. That is, it is governed by the fundamental laws of physics, in

particular, the Heisenberg uncertainty principle. In most literature "shot noise" refers to the noise associated with an electric current. Physically the noise is due to the random nature in which electrons in a current are emitted. Statistically the electron-arrival rate in a current also follows a Poisson distribution, and the mean-square current fluctuation is given by the following equation:

$$\bar{i}^2_{shot} = 2eI_{DC} \triangle B \tag{7.1}$$

Here I_{DC} is the average current; e is the electron charge; and $\triangle B$ is the measurement bandwidth.

Comparing this expression for the shot noise to the expression for the shot noise of light, one sees that the two forms are identical. The detection scheme used to detect squeezed light is simply a square-law photodetector that is sensitive only to the amplitude of the incoming light. The output current of the photodetector is directly proportional to the intensity of the incident light. Consequently, the detected current fluctuation is given by its shot noise provided that the incident light is also shot noise limited. Since the noise of light has no meaning until it is detected—as a current fluctuation—shot noise is, strictly speaking, a current noise only.

The relative intensity noise (RIN) characterizes fluctuations in the optical intensity emitted by a laser due to spontaneous emission[19]. It is defined as follows:

$$RIN = \frac{2 < |\Delta P(\omega_m)| >^2}{< P >^2} \Delta B \tag{7.2}$$

where $< P >$ denotes the mean optical power, and $P(\omega_m)$ is the noise spectral density evaluated a measurement frequency ω_m. RIN is measured as a noise current after the incident light is detected by a photodetector. The noise current is given by the following expression:

$$\bar{i}^2_{RIN} = (RIN){I_{DC}}^2 \Delta B \tag{7.3}$$

The detected RIN noise current is proportional to the square of the square of the dc photocurrent. Because of the square dependence, one expects that at sufficiently

high photocurrent levels the noise contribution from RIN will dominate over that from shot noise. The photocurrent level at which this condition takes place depends on the relative intensity noise defined in (7.2).

Thermal noise is another fundamental noise source. It is due to the thermal motion of electrons in a resistor and is given by the following expression:

$$\bar{i^2}_{thermal} = \frac{4kT}{R}\Delta B \tag{7.4}$$

Here R is the resistance of the resistor; T is the temperature; and k is the Boltzmann constant.

The noise power at the input of the rf amplifiers (prior to amplification) is given by the sum of the shot noise, the relative intensity noise, and the thermal noise due to the rf amplifier's input resistance R_{in}, which is 50Ω,

$$P_{priortoamp} = (4kT + 2eI_{DC}R_{in} + (RIN){I_{DC}}^2 R_{in})\Delta B \tag{7.5}$$

The rf amplifiers shown in Figure 16 also contribute excess noise. Depending on the type of the amplifier, the excess noise (referred to the input of the amplifier) due to the amplifier ranges from approximately 1.5dB to 4dB above thermal noise. The noise powers due to thermal noise and amplifier noise are often specified together as a "noise figure", which specifies the ratio (in dB's) between noise power at the amplifier output and the noise power due to a resistance R_{in} across the input terminals of the amplifier. The noise power at the output of the rf amplifiers thus includes an additional contrubution due to the excess noise from the amplifier itself:

$$P_{afteramp} = A_p(4kT10^{NF/10} + 2eI_{DC}R_{in} + (RIN){I_{DC}}^2 R_{in})\Delta B \tag{7.6}$$

Here A_p is the power gain by the amplifier, and NF denotes the noise figure. Since the output resistance of the rf amplifier is 50Ω, and the input resistance of the spectrum analyzer is also 50Ω, the rf amplifier and the spectrum analyzer are impedance matched, in which case the power delivered to the load (the spectrum analyzer) is $\frac{1}{4}$

of that given in (7.5),

$$P_{measured} = \frac{1}{4}A_p(4kT10^{NF/10} + 2eI_{DC}R_{in} + (RIN)I_{DC}{}^2R_{in})\Delta B. \qquad (7.7)$$

Specifically, the measured noise power given in the following section refers to the power delivered to the spectrum analyzer. The noise sources described so far all have no dependence on frequency (up to the terahertz range). In the frquency range of interest (20MHz to 1GHz) the measured noise is dominated by these noise sources.

7.2 Noise Measurement Results

As mentioned previously, the experiment employs a direct detection scheme. That is, amplitude-squeezed light is directly detected by a photodetector whose output is displayed on a spectrum analyzer after a certain amount of amplification. From the predictions given in Chapter 8, significant squeezing can be observed for measurement frequencies up to approximately 500MHz. It is therefore important that the system be shot noise limited in this frequency range. In the experimental setup most of the squeezed fundamental beam is reflected off the front facet of the crystal, and only a small fraction is transmitted through the crystal. Therefore, the squeezed fundamental field is detected from the reflected beam as shown in Figure 6. By contrast, the squeezed second harmonic field is detected from the transmitted beam. In this section, the noise measurement results for the fundamental and the second harmonic output fields are discussed and compared to those for the incident laser and for the reflected field in which the incident beam is reflected off a plain mirror instead of the monolithic cavity.

Figure 17 shows the noise of the incident laser as a function of the dc photocurrent generated by the photodetector. The noise is measured at a frequency of 160 MHz. The measured noise is compared to the expected total noise level (shotnoise + thermal noise + amplifier noise+RIN) (solid line) and to the shot noise level (dotted line). One sees that the measured noise agrees closely with the total predicted noise for dc

photocurrents up to 1.5mA. The parabolic dependence of the curve is due to RIN. A RIN level of 1.31×10^{-16}/Hz is determined by curve-fitting the experimental data to (7.6). The laser bias current is approximately 2.2 times that of the bias current at threshold. For photocurrents beyond 1.5mA, the measured noise, instead of continuing to increase parabolically, levels off somewhat. Note that, in combining different noise contributions, one adds up the powers associated with each noise contribution.

Figure 18 shows the noise of the laser beam reflected from a mirror. The schematic of the optical path is shown in Figure 19. The optical path is identical to the reflected beam from the front facet of the crystal. The measured noise agrees closely with the expected total noise for currents up to 3mA, the maximum current level at which the noise measurement is taken. The difference in the noise power levels at ($I_{DC} = 0$) between Figures 17 and 19 is due to the fact that different rf amplifiers, each with a slightly different gain and amplifier noise, are used. A RIN level of 1.18×10^{-16}/Hz is determined by curve-fitttting the date from Figure 19.

The noise of the reflected beam from the crystal is shown in Figure 20. Even at a moderate photocurrent level of 1mA, the measured noise is roughly 30dB, or a factor of 1000, beyond the expected noise at a frequency of 180MHz. Furthermore, the measured noise spectrum is no longer flat and has a slight bulge at low frequencies (Figure 21). Figure 22 shows the noise of the transmitted second harmonic field. As seen in the figure, there is significant excess noise at even very low dc photocurrent levels for the transmitted output beam.

The frequency selectivity of the cavity is hypothesized to be the cause of the excess noise, since the magnitude of the excess noise measured from the reflected beam from the cavity far exceeds those measured from the incident laser beam or in the reflected beam from a mirror. An attempt to account for the excess noise given the frequency selective nature of the cavity will be treated in section 9.4.

7.3 Mode Partition Noise

Mode partition noise refers to noise due to flucuations in the oscillating modes of a semiconductor laser. The semiconductor diode laser used in this experiment oscillates primarily in only one mode. The side modes are much reduced in intensity compared to the dominant mode. It has been shown that the fluctuations in the lasing mode can follow those in the non-lasing modes in a semiconductor laser[8]. That is, the total laser output contains less much less excess noise compared to the excess noise of each individual mode because of the correlations among intensity flucutations in the oscillating modes. However, if the laser output is passed through a frequency selective filter such that the various modes are attenuated by different amounts, the detailed balance among the partition noise components of the various modes is then disturbed, and the resulting laser output from the filter can be subject to significant excess noise. A simple semiquantitative model is presented in Appendix 2 to estimate the amount of excess noise power at the spectrum analyzer for the reflected field from the $KNbO_3$ cavity. The result will be compared to the excess noise power measured by the spectrum analyzer.

Chapter 8

Determination of Coupling Coefficient κ And Critical Power

Taking a second look at the expressions for the intensity fluctuations at the fundamental and at the second harmonic modes, one finds that squeezing is a sensitive function of the cavity parameters γ_1, γ_2, and κ. The techniques of determining γ_1, γ_2 and the measured results are discussed in Chapter 5. In this chapter the method of obtaining an experimental value for κ is discussed along with the measured results. A prediction of the critical power is calculated from the measured values for γ_1, γ_2, and κ. Furthermore, the amount of change in the critical power/critical frequency as a function of the amount of frequency detunings from the cavity resonance is numerically computed given the above cavity parameters.

8.1 Measurement of Coupling Coefficient κ

The coupling coefficient κ is given by the nonlinear optical coefficient d_{32} of the $KNbO_3$ crystal and by geometric factors. According to Drummond et. al.[5],

$$\kappa = 2d_{32}(\frac{\hbar\omega^3}{V\epsilon^3})^{1/2} \tag{8.1}$$

where $h = \hbar/2\pi$ is Planck's constant; ω is the optical angular frequency; and V is the mode volume inside the cavity. The d_{32} coefficient, obtained from literature[1], is $(1.81 \pm .03) \times 10^{-22}$F/V.

Using the above relationship κ is calculated to be $(2.17 \pm .03) \times 10^6/s$. The above calculation, however, requires knowledge of the beam waist inside the crystal. A more direct method involves measuring the conversion efficiency from the fundamental to the second harmonic mode to determine the coupling coefficient. In this method, the expression for κ as a function of the conversion efficiency is derived from the semiclassical equations of motion, and the result is given as follows and derived in Appendix 3:

$$\kappa = \gamma_2 \sqrt{\frac{2cn\hbar\omega_1 P_{cavity,2\omega}}{l P^2_{cavity,\omega}}} \tag{8.2}$$

Here $P_{cavity,\omega}$, $P_{cavity,2\omega}$ denote the power of the fundamental and second harmonic fields inside the cavity, and ω_1 is the angular frequency of the fundamental field. From the expression one sees that the coupling coefficient is also proportional to the cavity loss rate at the second harmonic wavelength. Since κ is a parameter that is independent of input power to the cavity, the ratio $P_{cavity,2\omega}/P^2{}_{cavity,\omega}$ must be a constant. Table 2 shows the measured ratio for three different input power levels and demonstrates that the ratio is independent of input power level.

Table 2. Conversion Efficiency Calculation

$P_{incident}$ (mW)	$P_{out,2\omega}$ (μW)	$P_{out,\omega}$ (μW)	$P_{cavity,2\omega}$ (mW)	$P_{cavity,\omega}$ (mW)	$\sqrt{P_{cavity,2\omega}/P^2{}_{cavity,\omega}}$
6.1	69.6	14.2	4.35	9.48	6.96
9.0	125	19.8	7.80	13.2	6.69
12.2	180	23.7	11.2	15.8	6.71

Experimentally, the fundamental and second harmonic frequencies are locked on resonance and phasematched to produce a stable second harmonic output beam. The fundamental and second harmonic output fields are separated by a filter, and their respective optical powers are measured. The power inside the cavity is related to the

output power by the power reflectivity of the cavity output facet:

$$P_{cavity,\omega} = \frac{P_{out,\omega}}{1 - R_{out,\omega}}$$

$$P_{cavity,2\omega} = \frac{P_{out,2\omega}}{1 - R_{out,2\omega}} \tag{8.3}$$

The measured ratio $P_{cavity,2\omega}/P^2{}_{cavity,\omega}$, along with knowledge of the cavity loss rate γ_2, determines κ, which is calculated to be $(2.74 \pm .13) \times 10^6/s$. This calculated value based on the conversion efficiency is in good agreement with the value determined from the theoretical expression for κ.

8.2 Dependence of Critical Power/Critical Frequency on Frequency Detunings

With knowledge of the cavity loss rates γ_1, γ_2 and the coupling coefficient κ, the critical power defined in Chapter 2 can be readily calculated. For $\gamma_1 = 6.32 \times 10^8/s$, $\gamma_2 = 1.95 \times 10^9/s$, and $\kappa = 2.74 \times 10^6/s$, the expected critical power is calculated to be 3.49mW, assuming zero frequency detunings. In practice, the the nonidealities associated with the frequency locking schemes may result in the frequency of the fields stabilized to a point slighly off the their respective resonances, resulting in small frequency detunings.

The formulas given in equations and apply only to the special case in which the frequencies of the fundamental and second harmonic fields are stabilized exactly on their respective cavity resonances. In practice, there are always a small amount of frequency detunings due to the nonidealities of the frequency locking electronics. To predict the effect small frequency detunings have on the critical power and frequency, the semiclassical equations of motion with non-zero detunings are solved, and critical powers with non-zero detunings are numerically calculated. Plots of the expected critical power and the corresponding critical frequency as a function of frequency detunings at the fundamental and second harmonic wavelengths are given in Figures

23a and 23b, respectively. Figures 24a and 24b give the same plots, except that zero detunings are assumed in the fundamental mode. For detunings of $\frac{1}{10}\gamma$, the upper limit for this experimental setup, the critical power increases only slightly, to 3.55mW. Therefore, the amount of frequency detunings present in the experiment is not expected to cause a significant shift in the critical power and critical frequency from the nondetuned values. Appendix 4 details the derivations for the critical power and frequency for zero detunings and the algorithm for numerically solving for the critical power and frequency with non-zero frequency detunings.

8.3 Experimental Determination of Critical Power

From the discussion in Chapter 2, the critical pump power is the power level above which self-pulsing oscillations take place and the linearized analysis from which the intensity fluctuation spectrums are derived no longer applies. Also, the amount of achievable squeezing improves as the input power is increased until the critical power level is reached. Hence, the input power for optimum squeezing is one just under the critical power level. From the previous section, a calculation of the input power level yields 3.49mW with zero detunings. This power level is certainly within the capability of the diode laser in use, which is capable of delivering approximately 20mW of input power to the cavity. Experimentally, one looks for the critical power by raising the input power until evidence of oscillation is detected. In this experiement the photodetector output of either the reflected field or the transmitted field is displayed on a spectrum analyzer. One then looks for oscillations in the frequency range within which the critical oscillation frequency is predicted to lie. The experimental setups are identical to the setups for noise detection (Chapter 7) and are shown in Figure 16. No evidence of oscillation has been observed in either the reflected field or the transmitted field spectrum for input powers up to 20mW. For the reflected field, where the large amounts of optical power available provide a more promising setting for detecting any oscillations, the enormous excess noise has probably swamped out any evidence of oscillations. For the transmitted field, the limited optical power makes it likely

that any oscillations would be dwarfed under the presence of other noise sources, i.e. thermal noise, amplifier noise, and frequency partition noise.

An attempt was made to reduce the excess noise from the reflected field by reducing the linewidth of the semiconductor laser via optical feedback. Two schemes shown in Figures 25a and 25b have been attempted. In the first a small portion of the laser output is diverted by a beam splitter onto a mirror. The mirror is adjusted to reflect the beam directly back into the laser. In the second scheme a confocal Fabry-Perot cavity instead of a mirror is used[12] [3] [13]. As shown in Figure 25b, the Fabry-Perot cavity is aligned off axis such that the reflected field amplitude is maximized at the resonance frequency of the Fabry-Perot cavity. Both schemes result in a reduction of the laser linewidth. The first scheme also results in a reduction of approximately 10dB in the excess noise power of the reflected field for frequencies up to 50MHz. However, the excess noise actually increases for higher frequencies. Since the critical oscillation frequency is predicted to be around 400MHz, the slight reduction in excess noise power below a frequency of 50MHz is not expected to increase the likelihood of observing the critical oscillation. Experimentally, no evidence of oscillation was observed with the linewidth reduction schemes.

Chapter 9

Detection Of Amplitude Squeezing

In this chapter the amount of achievable squeezing for the $KNbO_3$ monolithic cavity is discussed. The amount of achievable squeezing is based on the cavity parameters measured experimentally. From Chapter 2 the intensity fluctuation spectrum is expressed as a function of meausurement frequency Ω and plotted in Figure 26a using the experimentally determined parameters γ_1, γ_2, and κ. The plot assumes that the input power to the cavity is at the critical power of 3.49mW. According to Figure 27a, optimum squeezing occurs for measurement frequencies between 500 and 700MHz. A 31% reduction in intensity fluctuations below shot noise is predicted for the fundamental mode at a measurement frequency of 590MHz. For the second harmonic mode the best squeezing is achieved for measurement frequencies under 400MHz, where reduction in the intensity fluctuation of as much as 79% is predicted.

The intensity fluctuation spectrums for input powers at 10% and 1% of the critical power are plotted in Figures 26b and 26c, respectively. At the lower input powers the amount of squeezing is reduced at both the fundamental and second harmonic wavelengths. As seen from Figures 26b and 26c, the frequencies at which optimum squeezing is obtained are also reduced as the input power is decreased. At sufficiently low input power, the best squeezing is achieved at dc for both wavelengths. Further decrease in the input power results in reduction in the squeezing "bandwidth". That

is, the frequency above which the intensity fluctuation asymptotically approaches the shot-noise level. Figure 27a and 27b show the squeezing spectrum as a function of input power for fixed measurement frequencies. At the second harmonic wavelength (Figure 27a), the amount of squeezing decreases monotonically with increasing input power. At the fundamental wavelength (Figure 27b), however, the amount of achievable squeezing has a maximum. The location of the maximum is a function of the measurement frequency. Figure 28 shows a plot of the frequency at which squeezing is maximized as a function of input power. The results obtained are self-consitent with the conclusions derived from Figures 26b and 26c. Shown in Figure 27c is a plot of the amount of achievable squeezing as a function of input power, regardless of measurement frequencies. At the second harmonic wavelength, the achievalbe squeezing scales inversely with input power. At the fundamental wavelength, the amount of achievable squeezing is largely insensitive to input power. From the above calculations one can conclude that to optimize the amount of squeezing at the second harmonic wavelength, it is imperative to set the input power close to the critical power. At the fundamental wavelength, the input power level is not a crucial experimental parameter as far as achieving optimum squeezing is concerned. However, for other reasons such as noise performance discussed in Chapter 7, it is generally desirable to operate at an input power close to the critical power.

The enormous frequency partition noise present in the output fields of the cavity renders it impossible to detect amplitude squeezing using the the current setup. As discussed in Chapter 7 the frequency partition noise arises from the imbalance in the noise distribution between the main mode and the longitudinal sidemodes of the semiconductor laser. One of the possible future modifications to the current setup is to replace the semiconductor laser with a "quieter" laser source, such as a titanium sapphire laser.

Chapter 10

Conclusion

An experimental setup aimed at generating squeezed light via second harmonic generation from a monolithic potassium niobate cavity was constructed. Active stabilization of both the fundamental and second harmonic frequencies to their respective cavity resonance frequencies was successfully implemented. The cavity loss parameters γ_1, γ_2, at the fundamental and second harmonic, and the nonlinear conversion constant κ were determined from measurements of the bandwidth of the cavity at the two frequencies and the conversion efficiency to the second harmonic. From the cavity parameters the critical power and frequency can be calculated and used to predict the achievable amount of amplitude squeezing as functions of measurement frequency and input power. Table 3 provides a summary of the experimental results obtained in this work. The results show that from the cavity design one expects to observe significant amplitude squeezing at both wavelengths.

Expressions for the critical power and frequency as a function of cavity detunings were derived. These results do not appear in the literature but are important for relating theory to actual experimental conditions.

Table 3. Summary of Results

Item	Result
γ_1 Bandwidth(fundamental)	$(6.32 \pm .57) \times 10^8$/s (201 ± 18)MHz
γ_2 Bandwidth(second harmonic)	$(1.95 \pm .05) \times 10^9$/s (620 ± 15)MHz
κ	2.74×10^6/s
P_{crit} (predicted, no detuning)	3.49mW
Maximum predicted squeezing at P_{crit} (fundamental)	31%
Maximum predited squeezing at P_{crit} (second harmonic)	79%
Maximum length of time laser frequency remains locked	>6 hours
Maximum length of time second harmonic intensity remains locked	≈2 hours

An investigation of the noise of the output beams from the cavity reveals an enormous amount of excess noise in the reflected beam from the cavity. The enormity of this excess noise prevented experimental observation of amplitude squeezing with the current setup.

This excess noise can be attributed to the mode partition noise inherent in semiconductor diode lasers. Therefore, despite its compact size and relative inexpensiveness, the diode laser is not suitable as a source for amplitude squeezed light. Nevertheless, the low critical power calculated based on the measured cavity parameters suggests that the monolithic $KNbO_3$ cavity remains an attractive choice for the generation of squeezed light from a low-power laser source.

Bibliography

[1] J. C. Baumert, J. Hoffnagle, and P. Gunter. Nonlinear optical effects in $KNbO_3$ crystals at $Al_xGa_{1-x}As$, dye, ruby, and Nd:YAG laser wavelengths. In *SPIE Volume 492 ECOOSA '84*, Amsterdam, the Netherlands, 1984.

[2] G. C. Bjorklund and M. D. Levenson. Frequency modulation (fm) spectroscopy. *Applied Physics B*, 32:145, 1983.

[3] B. Dahmani, L. Hollberg, and R. Drullinger. Frequency stabilization of semiconductor lasers by resonant optical feedback. *Journal of Optical Society of America B*, 12:876, 1987.

[4] T. Debuisschert, S. Reynaud, A. Heidmann, E. Giacobino, and C. Fabre. Observation of large quantum noise reduction using an optical parametric oscillator. *Quantum Optics*, 1:3, 1989.

[5] P. D. Drummond, K. J. McNeil, and D. F. Walls. Non-equilibrium transitions in sub/second harmonic generation. 1. semiclassical theory. *Optica Acta*, 27(3):321, 1980.

[6] H. A. Haus. *Waves and Fields in Optoelectronics*. Prentice-Hall, Inc., Englewood Cliffs, N.J., 1984.

[7] A. Heidmann, R. J. Horowicz, S. Reynaud, E. Giacobino, and C. Fabre. Observation of quantum noise reduction on twin laser beams. *Physical Review Letters*, 59(22):2555, 1987.

[8] C. H. Henry, P. S. Henry, and M. Lax. Partition fluctuatios in nearly single-longitudinal-mode lasers. *Journal of Lightwave Technology*, LT-2(3):209, 1984.

[9] D. Hills and J. L. Hall. Response of a fabry-perot cavity to phase modulated light. *Rev. Sci. Instrum.*, 58(8):1406, 1987.

[10] R. J. Horowicz. Quantum correlation between fundamental and second harmonic in shg. *Europhysics Letters*, 10(6):537, 1989.

[11] P. Kürtz, R. Paschotta, K. Fielder, A. Sizmann, G. Leuchs, and J. Miynek. Squeezing by second harmonic generation in a monolithic resonator. *Applied Physics B*, 55:216, 1992.

[12] W. D. Lee and J. C. Campbell. Frequency stabilization of an external-cavity diode laser. *Applied Physics Letters*, 57(21):2181, 1990.

[13] H. Li and H. R. Telle. Efficient frequency noise reduction of gaalas semiconductor lasers by optical feedback from an external high-finesse resonator. *IEEE Journal of Quantum Electronics*, 25(3):257, 1989.

[14] S. Machida, Y. Yamamoto, and Y. Itaya. Observation of amplitude squeezing in a constant-current-driven semiconductor laser. *Physical Review Letters*, 58:1000, 1987.

[15] M. W. Maeda, P. Kumar, and J. H. Shapiro. Observation of squeezed noise produced by four-wave mixing in sodium vapor. *Optics Letters*, 12(3):161, 1987.

[16] J. Mertz, A. Heidmann, C. Fabre, E. Giacobinao, and S. Reynaud. Observation of high intensity sub-poissonian light using an optical parametric oscillator. *Physical Review Letters*, 64(24):2897, 1990.

[17] C.D. Nabors and R.M. Shelby. Two-color squeezing and sub-shot noise signal recovery in doubly resonant optical parametric oscillators. *Physical Review A*, 42(1):556, 1990.

[18] S.F. Pereira, M. Xiao, H.J. Kimble, and J.L. Hall. Generation of squeezed light by intracavity frequency doubling. *Physical Review A*, 38(9):4931, 1988.

[19] K. Petermann. *Laser Diode Modulation and Noise.* Kluwer Academic Publishers, Boston, 1988.

[20] R. V. Pound. *Rev. Sci. Instrum.*, 17:490, 1946.

[21] M. G. Raizen, L. A. Orozco, M. Xiao, T. L. Boyd, and H. J. Kimble. Squeezed-states generation by the normal modes of a coupled system. *Physical Review Letters*, 59(2):198, 1987.

[22] E. A. Saleh and M. C. Teich. Can the channel capacity of a light-wave communications system be increased by the use of photon-number-squeezed light? *Physical Review Letters*, 58:2656, 1987.

[23] R. M. Shelby, M. D. Levenson, S. H. Perlmutter, R. G. DeVoe, and D. F. Walls. Broad-band parametric deamplification of quantum noise in an optical fiber. *Physical Review Letters*, 57(6):691, 1986.

[24] A. Sizmann, R.J. Horowicz, G. Wagner, G. Leuchs, and J. Miynek. Observation of amplitude squeezing of the up-converted mode in second harmonic generation. *Optics Communications*, 80(2):138, 1990.

[25] R. E. Slusher, P. Grangier, A. LaPorta, B. Yurke, and M. J. Potasek. Pulsed squeezed light. *Physical Review Letters*, 59(22):2566, 1987.

[26] R. E. Slusher, L. W. Hollberg, B. Yurke, J. C. Mertz, and J. F. Valley. Observation of squeezed states generated by four-wave mixing in an optical cavity. *Physical Review Letters*, 55(22):2409, 1985.

[27] P. R. Tapster, J. G. Rarity, and J. S. Satchell. Use of parametric down-conversion to generate sub-poissonian light. *Physical Review A*, 37(8):2963, 1988.

[28] M. C. Teich and E. A. Saleh. Squeezed and anibunched light. *Physics Today*, 6:26, 1990.

[29] L. A. Wu, H. J. Kimble, J. L. Hall, and H. Wu. Generation of squeezed states by parametric down conversion. *Physical Review Letters*, 57(20):2520, 1986.

[30] L.A. Wu, M. Xiao, and H.J. Kimble. Squeezed states of light from an optical parametric oscillator. *Journal of Optical Society of America B*, 4(10):1465, 1987.

[31] A. Yariv. *Quantum Electronics.* John Wiley and Sons, New York, 1989.

Appendix A

I. Derivation of Expression For Cavity Loss Rate γ

The derivation below largely follows that given in Yariv's text[31, p. 147]. Consider the intensity I of an optical beam. Let I_f denote the intensity after one roundtrip through the cavity:

$$I_f = R_1 R_2 e^{-2\alpha l} I_i = e^{-2(\alpha l - ln\sqrt{R_1 R_2})} I_i \tag{.1}$$

Recall from Chapter 7 that α is the distributed loss per unit length; R_1, R_2 are the mirror reflectivities of the input and output facets, respectively; and l is the cavity length.

If one defines the loss per pass (as opposed to the loss per roundtrip) of the beam to be L, such that

$$L = 1 - e^{-(\alpha l - ln\sqrt{R_1 R_2})} \tag{.2}$$

the power loss per unit time of the beam is $L \times \frac{c}{nl}$ where n is the index of the medium.

The cavity loss rate γ defined in (5.1) can also be defined by

$$\frac{d}{dt} I = -2\gamma I \tag{.3}$$

since intensity is proportional to the square of the field. Hence, the power loss per unit time is

$$2\gamma = \frac{c}{nl} L \tag{.4}$$

Substituting (.2) into (.4), one obtains

$$\gamma = \frac{c}{2nl}[1 - e^{-(\alpha l - ln\sqrt{R_1 R_2})}] \tag{.5}$$

For the case of $L \ll 1$,

$$L \approx 1 - (1 - \alpha l + ln\sqrt{R_1 R_2}) = \alpha l - ln\sqrt{R_1 R_2} \tag{.6}$$

Under this approximation,

$$\gamma = \frac{c}{2n}(\alpha - \frac{1}{l} ln\sqrt{R_1 R_2}) \tag{.7}$$

which is identical to (5.2)

II. Relating γ to the Cavity Bandwidth $\Delta\nu_{FWHM}$

The Q-factor of the resonator is defined as

$$Q = \frac{\omega \mathcal{E}}{P} = -\frac{\omega \mathcal{E}}{d\mathcal{E}/dt} \tag{.8}$$

Here $\mathcal{E}$ refers to the stored energy, and P refers to the dissipated power. Since the energy inside the resonator is proportional to its intensity,

$$|\frac{\mathcal{E}}{d\mathcal{E}/dt}| = |\frac{I}{dI/dt}| = \frac{1}{2\gamma} \tag{.9}$$

One thus obtains,

$$Q = \frac{\omega}{2\gamma} \tag{.10}$$

The full-width-at-half-maximum bandwidth $\Delta\nu_{FWHM}$ is given in terms of Q as

$$\Delta\nu_{FWHM} = \nu/Q = \frac{\gamma}{\pi} \tag{.11}$$

One gets, from (.11),

$$\gamma = \pi \Delta\nu_{FWHM} \tag{.12}$$

which is identical to (5.3)

Appendix B

Estimation of Mode Partition Noise

Following the treatment used in Henry et. al.[8], a linearized model is used to estimate the amount of excess noise power at the spectrum analyzer, following detection of the reflected laser light from the cavity. The calculation assumes a modest input optical power of 1.6mW and mode intensity fluctuation levels typical of diode lasers. For simplicity one assumes that only two modes—the main mode and the first sidemode—of the diode laser contribute to the mode partition noise.

The intensities of the two modes are denoted as follows:

$$I(t) = I_o + \Delta I(t)$$

$$J(t) = J_o + \Delta J(t) \tag{.13}$$

$I(t)$, $J(t)$ are the intensities of the main mode and side mode, respectively, and $\Delta I(t)$, $\Delta J(t)$ are the intensity fluctuations in each mode. In the following analysis it is also assumed that $I_o \gg J_o$ and $I_o \gg \Delta I, \Delta J$. Henry et. al.[8] showed that $\Delta I(t) = -\Delta J(t)$ using the simplified model. This requires that the total output power is a constant in time:

$$I(t) + J(t) = I_o + J_o \tag{.14}$$

The above conclusion is not true, strictly speaking, since it does not account for the the excess noise associated with the total laser output (RIN) observed experimentally. However, since the excess noise of each mode far exceeds that of the total laser output for typical diode lasers, the assumption of a constant total power is considered reasonable.

The monolithic $KNbO_3$ cavity serves as a frequency selective filter. When the laser

is locked on resonance, the sidemode power is assumed to be completely reflected, but only a fraction of the incident main mode power is reflected. The ratio of the reflected power to the incident power is measured to be .72. The reflected power from the cavity can thus be expressed as

$$P_{reflected} = .72I + J = .72(I_o + \Delta I) + (J_o + \Delta J)$$

Using the assumption $\Delta J = -\Delta I$, one gets

$$P_{reflected} = (.72I_o + J_o) - .28\Delta I \tag{.15}$$

The reflected power thus contains a fluctuating term that is proportional to the intensity fluctuation of the main mode only. The excess noise power of the reflected field is thus

$$P_{noise,opt} = .28\Delta I \tag{.16}$$

Referring to the noise detection scheme given in Figure 17, the fluctuation in the intensity of the reflected field is detected by a photodetector, amplified by an rf-coupled amplifier, and displayed on the spectrum analyzer. The noise power measured at the spectrum analyzer can be expressed as follows:

$$P_{noise,elect}/\Delta B = \frac{1}{4\Delta B}(.28)[r_{resp}\Delta I]^2 R_{in} G_p \tag{.17}$$

Here r_{resp} is the responsivity of the photodetector; R_{in} is the input impedance of the rf-coupled amplifier; G_p is the power gain of the rf amplifier; and ΔB is the measurement bandwidth of the spectrum analyzer. The fractional intensity fluctuaion of the lasing mode is on the order of 10^{-3} for an input optical power of 1.6 mW. That is, $\frac{\Delta I}{I_o} \approx 10^{-3}$. Using this value for $\frac{\Delta I}{I_o}$, we obtain an estimate for the excess noise power at the spectrum analyzer and compare it to the value measured experimentally.

For an input optical power of 1.6 mW, $\Delta I = 16\mu$W. Given that $r_{resp} = .613$ A/W, $R_{in} = 50\Omega$, $G_p = 57$ dB, and $\Delta B = 741$ kHz, the noise power is calculated from (.16) to be -86 dBm/Hz. This estimated noise power is compared to the measured noise

power of approximately -85 dBm/Hz given in Figure 20. According to the presently used model, as the input optical power increases, the power fluctuation is correspondingly increased, giving rise to enhanced excess noise at higher photocurrents. This behavior is not observed experimentally. As shown in Figure 20, the excess noise power saturates to approximately -80 dBm/Hz for for photocurrent levels above 1 mA.

From the above calculations one finds that to within an order of magnitude the estimated excess noise power agrees with the measured excess noise power for an input optical power of 1.6 mW. The calculated result shows that mode partition fluctuations do indeed produce enormous excess noise power when the laser output field is filtered.

Appendix C

Determining κ From Amount of Second Harmonic Conversion

We first derivee a relationship between the normalized field variable α and the physical power P.

The intensity of a plane wave propagating in a medium of index n is

$$I =< S >= \frac{E^2}{2\eta} \tag{.18}$$

where E is the electric field, and $\eta = \sqrt{\frac{\epsilon}{\mu_o}}$ is the characteristic impedance. Since the index n is related to the permittivity ϵ by $\epsilon = n^2\epsilon_o$, (.18) can be expressed as

$$I =< S >= \frac{1}{2}cn\epsilon_o|E|^2 \tag{.19}$$

From (2.10) the electric field $\mathcal{E}$ is related to the normalized field amplitude α by

$$\mathcal{E} = j\sqrt{\frac{2h\nu}{\epsilon_o V}}\alpha$$

Substituting (2.10) into (.19), one obtains

$$I = \frac{cn\hbar\omega}{V}|\alpha|^2 \tag{.20}$$

The power, obtained by integrating over the area of the beam, is given in terms of the normalized field variable α as

$$P = \frac{cn\hbar\omega}{l}|\alpha|^2 \tag{.21}$$

The power P derived above denotes the circulating power inside the cavity, and l is the cavity length.

In the steady state, the time derivatives in the equations of motion given in (2.9) vanish. That is, $\frac{d}{dt}\alpha_1 = \frac{d}{dt}\alpha_2 = 0$. Assuming further that there are no frequency detunings, $\Delta_1 = \Delta_2 = 0$, κ can be expressed as a function of the normalized field variables:

$$\kappa = 2\gamma_2 \frac{|\alpha_{20}|}{{\alpha_{10}}^2} \tag{.22}$$

Here α_{10} and α_{20} denote the steady-state normalized field amplitudes at the fundamental and second harmonic frequencies, respectively. By expressing $|\alpha_{10}|$ and $|\alpha_{20}|$ in terms of physical powers using (.21), (.22) becomes

$$\kappa = \gamma_2 \sqrt{\frac{2cn\hbar\omega_1 P_{cavity,2\omega}}{l{P^2}_{cavity,\omega}}} \tag{.23}$$

where $P_{cavity,\omega}$ and $P_{cavity,2\omega}$ denote the optical power inside the cavity at the fundamental and second harmonic wavelengths, respectively.

Appendix D

I. Derivation of Expression For Critical Power With No Frequency Detunings

From the equations of motion given in (2.9), expressions for small perturbations $\delta\alpha_1$, $\delta\alpha_2$ around steady state values α_{10} and α_{20} can be obtained (with the additional assumption of zero frequency detunings Δ_1, Δ_2):

$$\frac{d}{dt}\delta\alpha_1 = -\gamma_1\delta\alpha_1 + \kappa\alpha_{20}\delta{\alpha_1}^* + \kappa\alpha_{10}\delta\alpha_2$$

$$\frac{d}{dt}\delta{\alpha_1}^* = \kappa{\alpha_{20}}^*\delta\alpha_1 - \gamma_1\delta{\alpha_1}^* + \kappa\alpha_{10}\delta{\alpha_2}^*$$

$$\frac{d}{dt}\delta\alpha_2 = -\kappa\alpha_{10}\delta\alpha_1 - \gamma_2\delta\alpha_2$$

$$\frac{d}{dt}\delta{\alpha_2}^* = -\kappa{\alpha_{10}}^* - \gamma_2\delta{\alpha_2}^* \qquad (.24)$$

Assume $\delta\alpha_1$, $\delta\alpha_2 \propto e^{\lambda t}$, where λ are the eigenvalues of the 4th-order matrix given above. Solving for the eigenvalues, one obtains

$$\lambda_1, \lambda_2 = -\frac{1}{2}[-\kappa|\alpha_{20}| + \gamma_1 + \gamma_2] \pm \frac{1}{2}[(-|\kappa\alpha_{20}| + \gamma_1 - \gamma_2)^2 - 4|\kappa\alpha_{10}|^2]^{\frac{1}{2}}$$

$$\lambda_3, \lambda_4 = -\frac{1}{2}[-\kappa|\alpha_{20}| + \gamma_1 + \gamma_2] \pm \frac{1}{2}[(|\kappa\alpha_{20}| + \gamma_1 - \gamma_2)^2 - 4|\kappa\alpha_{10}|^2]^{\frac{1}{2}} \qquad (.25)$$

These eigenvalues are used to determine the stability of the solutions.

Under the conditions of steady state and zero frequency detunings:

$$\frac{d\alpha_1}{dt} = 0 = -\gamma_1\alpha_{10} + \kappa{\alpha_{10}}^*\alpha_{20} + \epsilon_1$$

$$\frac{d\alpha_2}{dt} = 0 = -\gamma_2\alpha_{20} - \frac{1}{2}\kappa{\alpha_{10}}^2 \qquad (.26)$$

Rearranging, one gets

$$\epsilon_1 = \gamma_1 \alpha_{10} - \kappa \alpha_{10}{}^* \alpha_{20} \tag{.27}$$

$$\alpha_{10}{}^2 = -\frac{2}{\kappa} \gamma_2 \alpha_{20} \tag{.28}$$

Multiplying (.27) by its own complex conjugate and then substituting (.28) into resulting expression, one obtains, after some algebraic manupulation, an expression relating the second harmonic field amplitude to the input pump power:

$$|\kappa \epsilon_1|^2 = -2\gamma_2 (\kappa \alpha_{20})^3 + 4\gamma_1 \gamma_2 (\kappa \alpha_{20})^2 - 2\gamma_1{}^2 \gamma_2 (\kappa \alpha_{20}) \tag{.29}$$

The expressions for λ_1, λ_2 become, upon substituting (.28) into (.25),

$$\lambda_1, \lambda_2 = -\frac{1}{2}[-\kappa|\alpha_{20}| + \gamma_1 + \gamma_2] \pm \frac{1}{2}[|\kappa \alpha_{20}|^2 + (\gamma_1 - \gamma_2)^2 - 2|\kappa \alpha_{20}|(\gamma_1 + 3\gamma_2)]^{\frac{1}{2}} \tag{.30}$$

For ϵ_1 small, $|\kappa \alpha_{20}|$ is small. In this regime λ_1, λ_2 contain negative real parts, and the solution of α_2 converges to α_{20} as $t \Longrightarrow \infty$. As $\kappa \alpha_{20} \Longrightarrow -(\gamma_1 + \gamma_2)$, the negative real parts of λ_1, λ_2 vanish, leaving purely imaginary parts:

$$\lambda_1, \lambda_2 = \pm i[\gamma_2 (2\gamma_1 + \gamma_2)]^{\frac{1}{2}} \tag{.31}$$

The magnitude of the purely imaginary parts of λ_1, λ_2 is the critical oscillation frequency:

$$\omega_{crit} = \sqrt{\gamma_2 (\gamma_1 + \gamma_2)} \tag{.32}$$

The pump power at which λ_1, λ_2 become purely imaginary is the critical pump power. Subsituting $\kappa \alpha_{20} = -(\gamma_1 + \gamma_2)$ into (.29), one gets

$$|\kappa \epsilon_{1c}|^2 = 2\gamma_2 (\gamma_1 + \gamma_2)(2\gamma_1 + \gamma_2)^2 \tag{.33}$$

Taking the square root and dividing by κ, one obtains the expression for the critical

pump power in terms of γ_1, γ_2, and κ:

$$|\epsilon_{1c}| = \frac{2\gamma_1 + \gamma_2}{\kappa}\sqrt{2\gamma_2(\gamma_1 + \gamma_2)} \tag{.34}$$

II. Algorithm for Determining Critical Power and Frequency With Nonzero Frequency Detunings

The linearized equations around the steady state solutions α_{10}, α_{20} with nonzero frequency detunings are

$$\delta\alpha_1 = -(\gamma_1 + i\Delta_1)\delta\alpha_1 + \kappa\alpha_{20}\delta\alpha_1^* + \kappa\alpha_{10}^*\delta\alpha_{20}$$

$$\delta\alpha_1^* = -(\gamma_1 - i\Delta_1)\delta\alpha_1^* + \kappa\alpha_{20}^*\delta\alpha_1 + \kappa\alpha_{10}\delta\alpha_2^*$$

$$\delta\alpha_2 = -(\gamma_2 + i\Delta_2)\delta\alpha_2 - \kappa\alpha_{10}\delta\alpha_1$$

$$\delta\alpha_2^* = -(\gamma_2 - i\Delta_2)\delta\alpha_2^* - \kappa\alpha_{10}^*\delta\alpha_1^* \tag{.35}$$

The eigenvalues of this 4th-order matrix equation are given by the roots of the following 4th order polynomial:

$$\lambda^4 + [2(\gamma_1 + \gamma_2)]\lambda^3 + [(\gamma_2{}^2 + \Delta_2{}^2) + 4\gamma_1\gamma_2 + (\gamma_1{}^2 + \Delta_1{}^2) + 2|\kappa\alpha_{10}|^2 - |\kappa\alpha_{20}|^2]\lambda^2$$

$$+[2\gamma_1(\gamma_2{}^2 + \Delta_2{}^2) + 2\gamma_2(\gamma_1{}^2 + \Delta_1{}^2) + 2|\kappa\alpha_{10}|^2(\gamma_1 + \gamma_2) - 2|\kappa\alpha_{20}|^2\gamma_2]\lambda$$

$$+(\gamma_1{}^2 + \Delta_1{}^2)(\gamma_2{}^2 + \Delta_2{}^2) + 2|\kappa\alpha_{10}|^2(\gamma_1\gamma_2 - \Delta_1\Delta_2) - |\kappa\alpha_{20}|^2(\gamma_2{}^2 + \Delta_2{}^2) + |\kappa\alpha_{10}|^4 \tag{.36}$$

Again, by assuming steady state, one can set the time derivates equal to zero in the equations of motion and obtain the following expression for α_{10} and ϵ_1:

$$\alpha_{10}{}^2 = -\frac{2}{\kappa}(\gamma_2 + i\Delta_2)\alpha_{20} \tag{.37}$$

$$\epsilon_1 = (\gamma_1 + i\Delta_1)\alpha_{10} + \kappa\alpha_{10}{}^*\alpha_{20} \tag{.38}$$

Taking the modulus of (.37), one obtains

$$|\alpha_{10}|^2 = \frac{2}{\kappa}\sqrt{\gamma_2{}^2 + \delta_2{}^2}|\alpha_{20}| \tag{.39}$$

Multiplying (.38) by its complex conjugate and substituting (.39) to eliminate α_{10}, one obtains an expression for $|\epsilon_1|^2$ as a function of $|\alpha_{20}|$,

$$|\epsilon_1|^2 = \frac{2}{\kappa}(\gamma_1{}^2 + \Delta_1{}^2)\sqrt{\gamma_2{}^2 + \Delta_2{}^2}|\alpha_{20}| + 4(\gamma_1\gamma_2 - \Delta_1\Delta_2)|\alpha_{20}|^2 + 2\kappa\sqrt{\gamma_2{}^2 + \Delta_2{}^2}|\alpha_{20}|^3 \tag{.40}$$

Note that (.40) is the same as (.29) except that frequency detuning terms are included.

Finally, one needs to relate the normalized pump field ϵ_1 (in units of inverse time) to the input optical power. From Drummond et. al.[5] the input power is related to ϵ_1 by the following equation:

$$P_{in} = \frac{\hbar\omega_1(\Delta t)|\epsilon_1|^2}{1 - R_{in}} \tag{.41}$$

where the roundtrip time Δt around the cavity is given by $\Delta t = \frac{2nl}{c}$. Here, ω_1 is the angular frequency of the optical field; R_{in} is the power reflectivity of the input facet; n is the index of refraction; and l is the cavity length. In this experiment, $\omega_1 = 2.19 \times 10^{15}/\text{s}$; $R_{in} = 0.9$; $n = 2.28$; and $l = 7.2$ mm. Substituting these values into (.41), one obtains

$$P_{in} = 2.52 \times 10^{-28}|\epsilon_1|^2(Watts) \tag{.42}$$

Given that the parameters γ_1, γ_2, and κ are already known, (.36), (.39), (.40), and (.42) enable one to compute the critical power as a function of frequency detuning by iteration. The procedure is outlined as follows:

1. Determine the critical power and frequency with no frquency detunings from (.32), (.34), and (.42). From (.28) and (.29), determine $|\alpha_{10}|$ and $|\alpha_{20}|$.

2. Using the values for $|\alpha_{10}|$ and $|\alpha_{20}|$ obtained in step 1, solve for the roots of (.36).

3. After examining the real and imaginary parts of the roots, increase P_{in} slightly

from the critical power with no frequency detunings. Recalculate $|\alpha_{10}|$ and $|\alpha_{20}|$ and solve for the roots of (.36) again to obtain a new set of roots (eigenvalues). Continue the iteration process until the real part of one of the conjugate pairs of roots vanish. The value of P_{in} for which this condition is satisfied is the new critical power. The imaginary part of the roots becomes the new critical frequency.

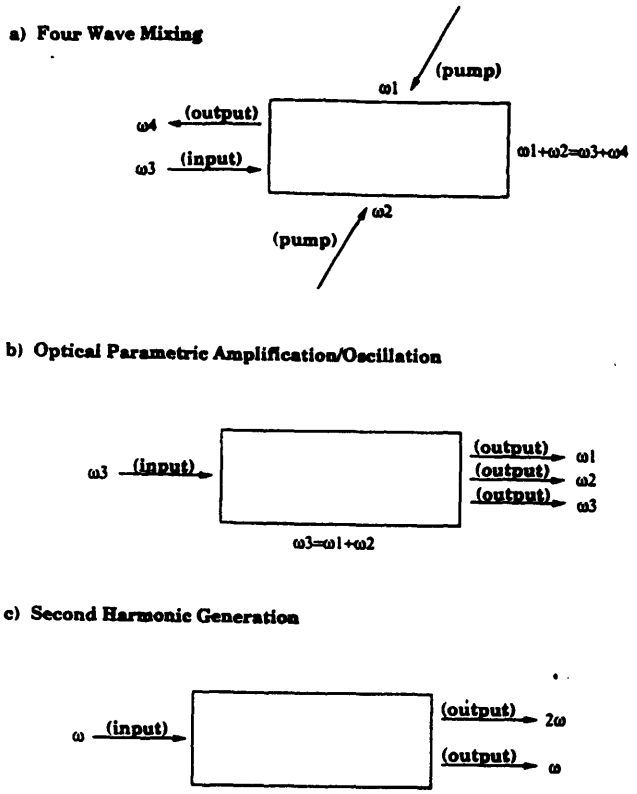

Figure 1. Three processes from which squeezing has been generated.

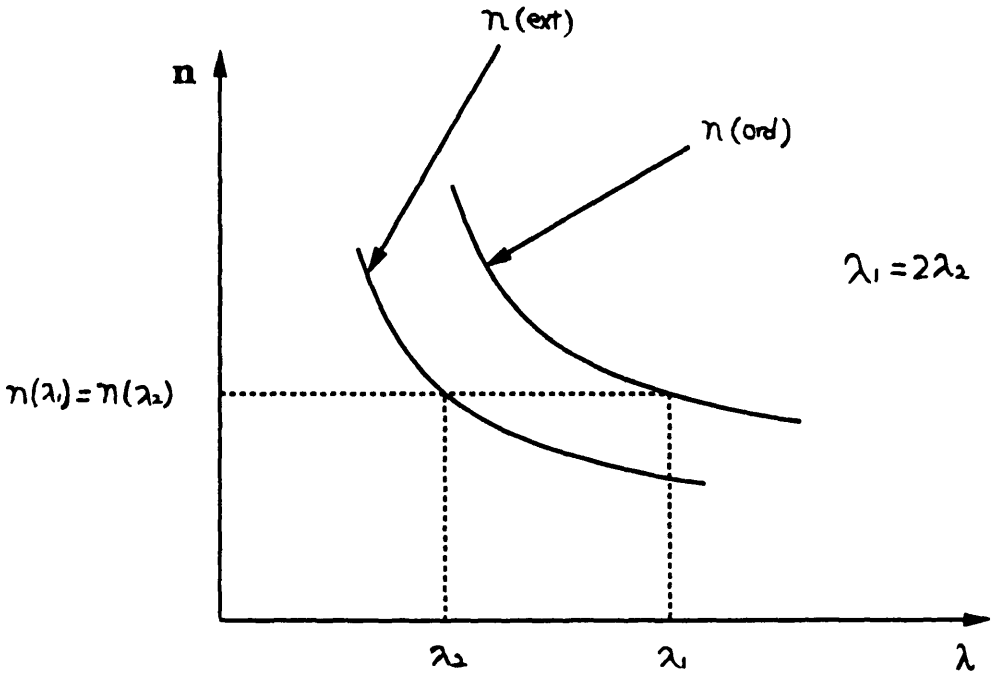

Figure 2. Dependence of index of refraction on wavelength for an anisotropic medium.

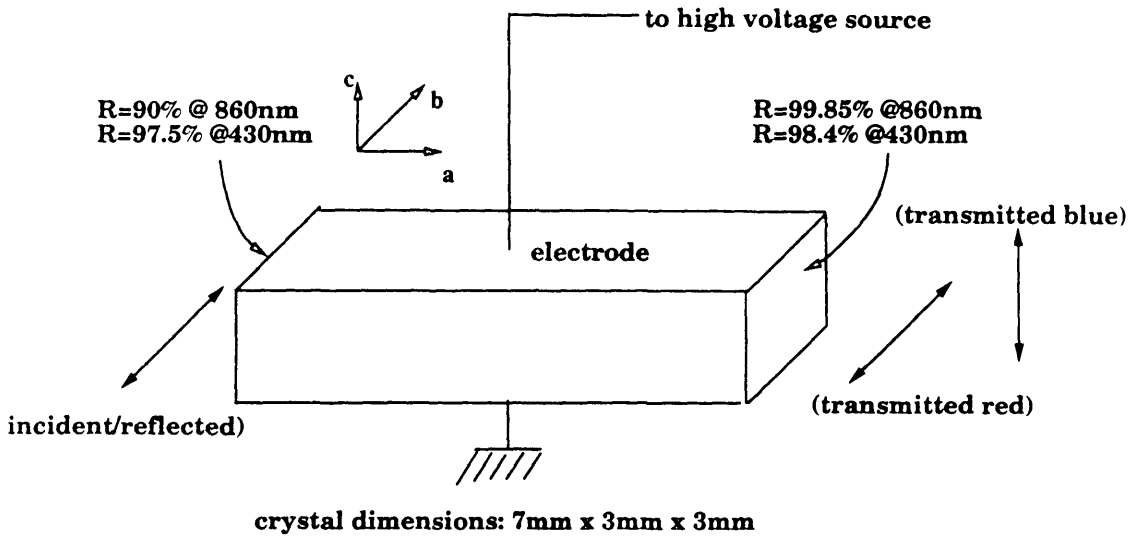

Figure 3. Doubly resonant monolithic cavity for second harmonic generation.

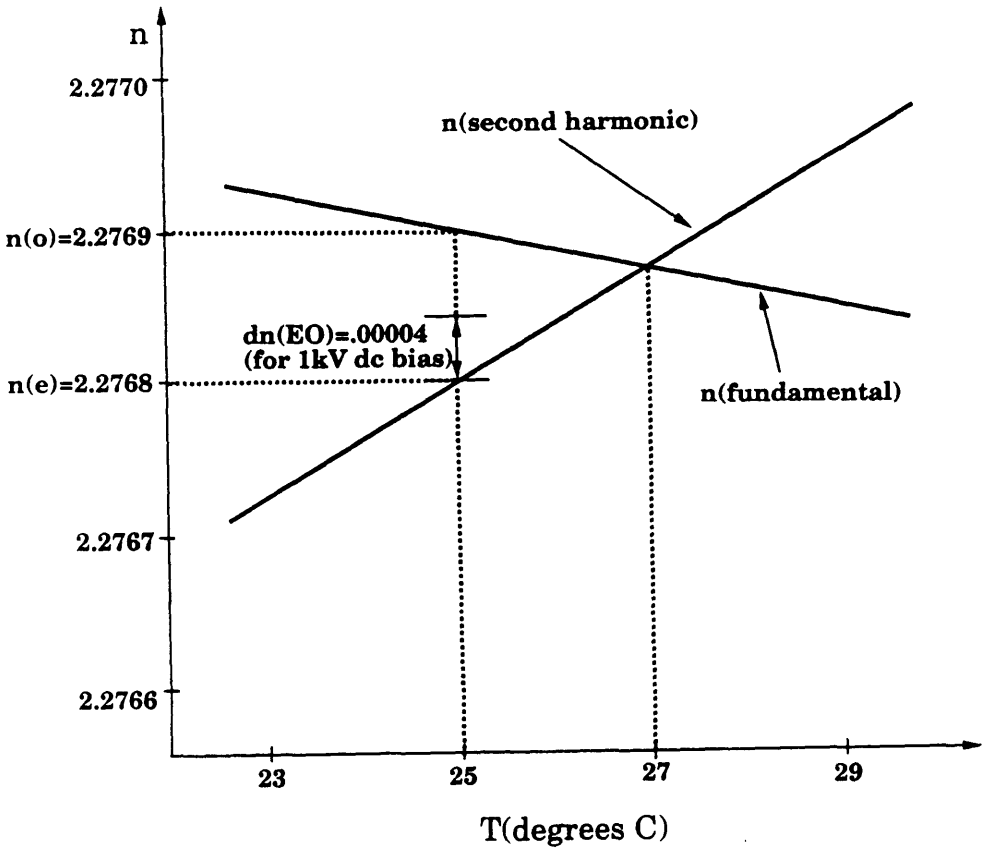

Figure 4. Phasematching by temperature and by electro-optic effect.

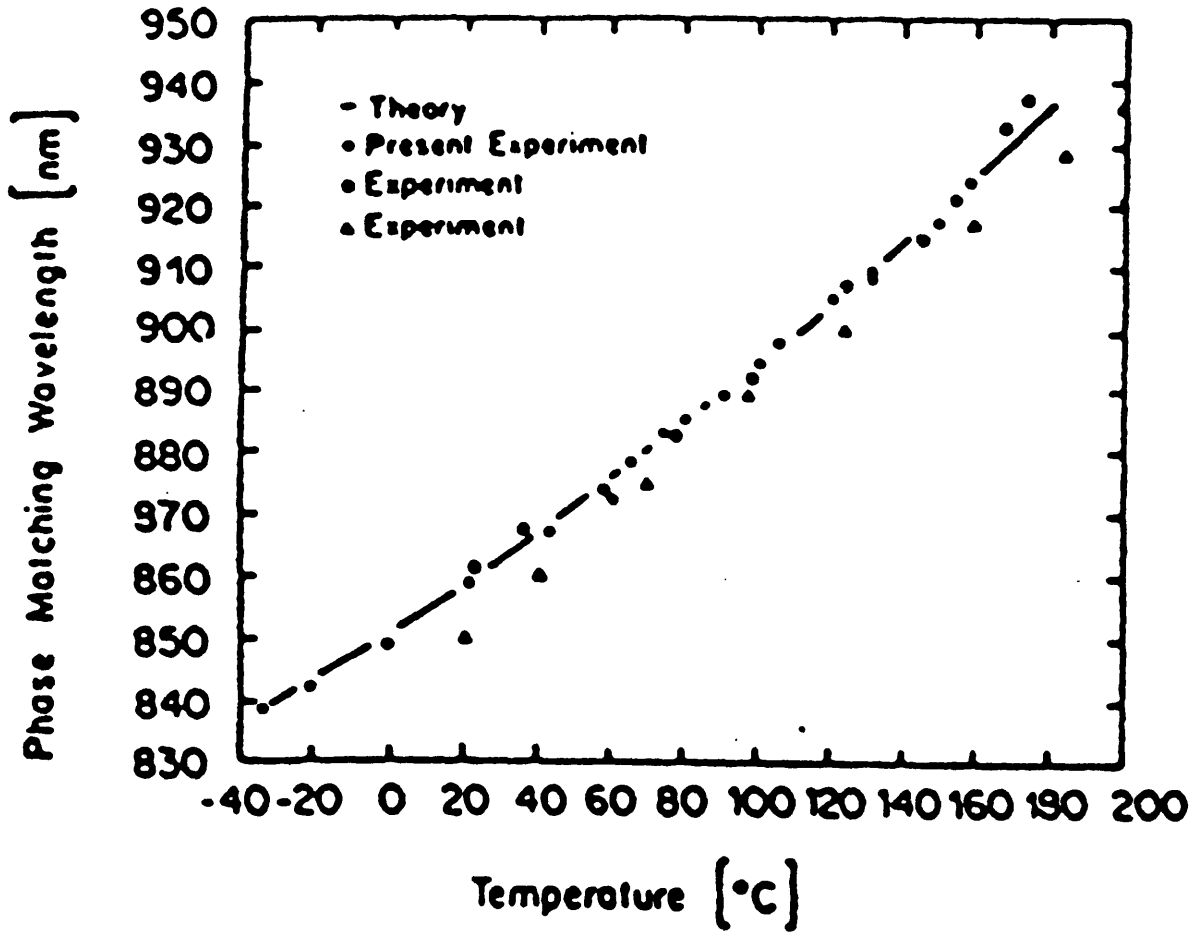

Figure 5. Temperature dependence of the phasematching wavelength for the nonlinear optical coefficient d_{32} of $KNbO_3$.

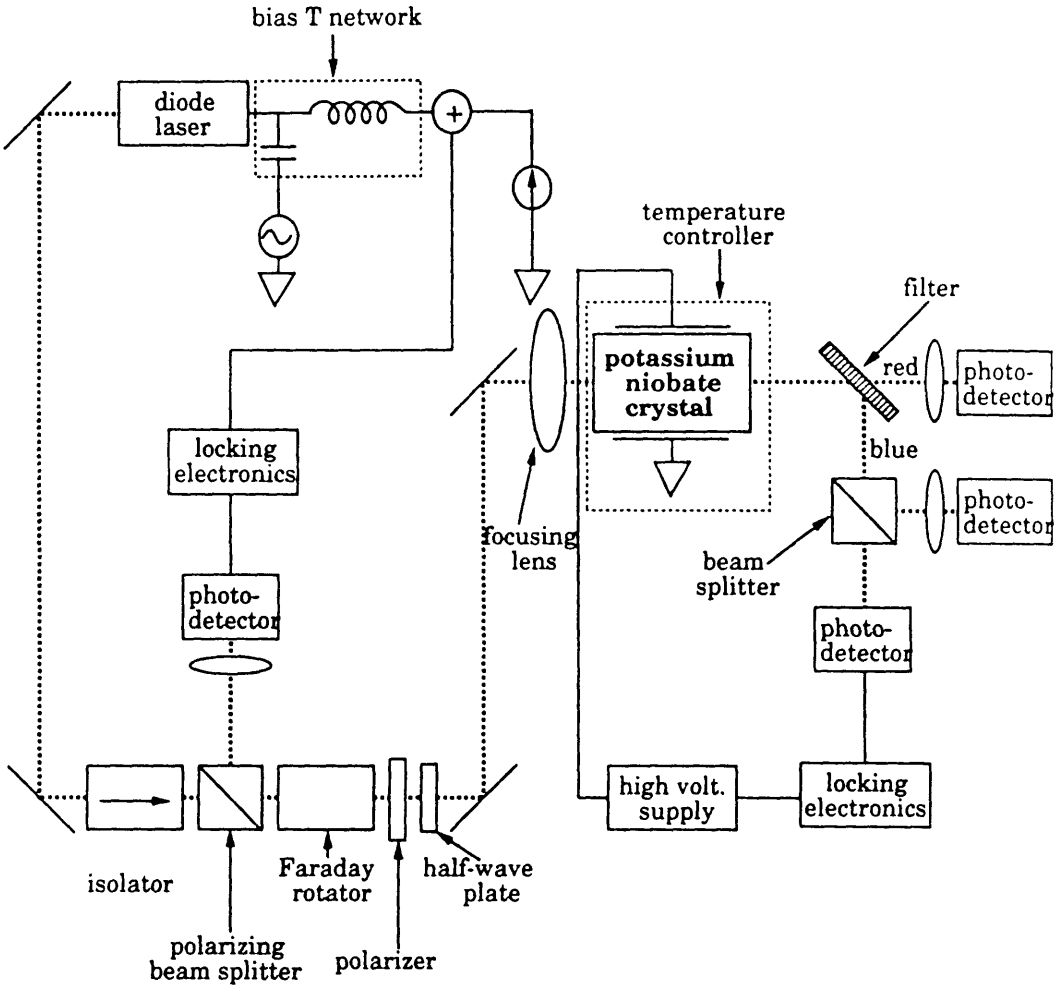

Figure 6. Experimental setup.

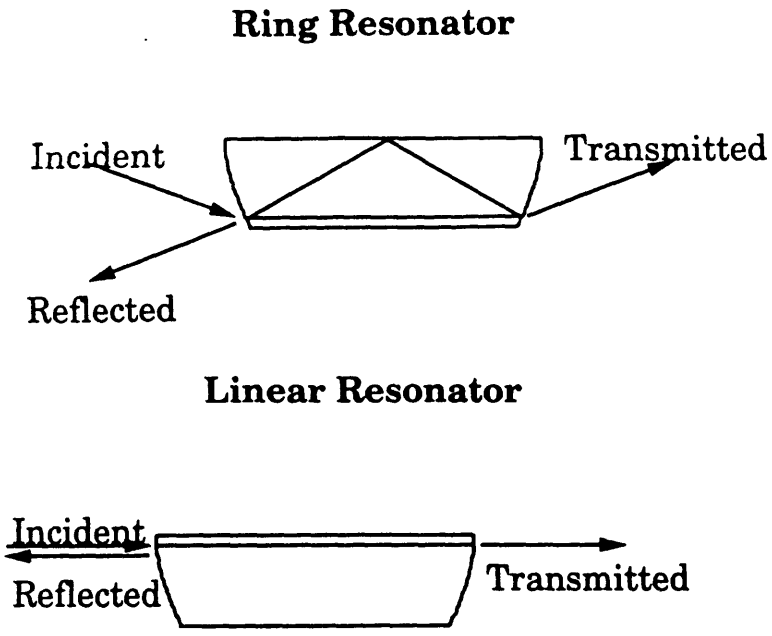

Figure 7. Two possible resonator configurations.

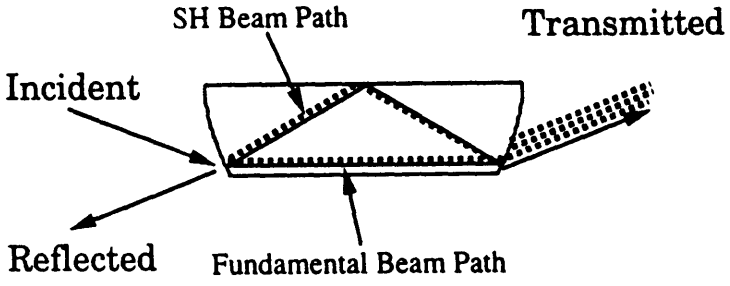

Figure 8. Nonoverlapping beam paths in the ring resonator.

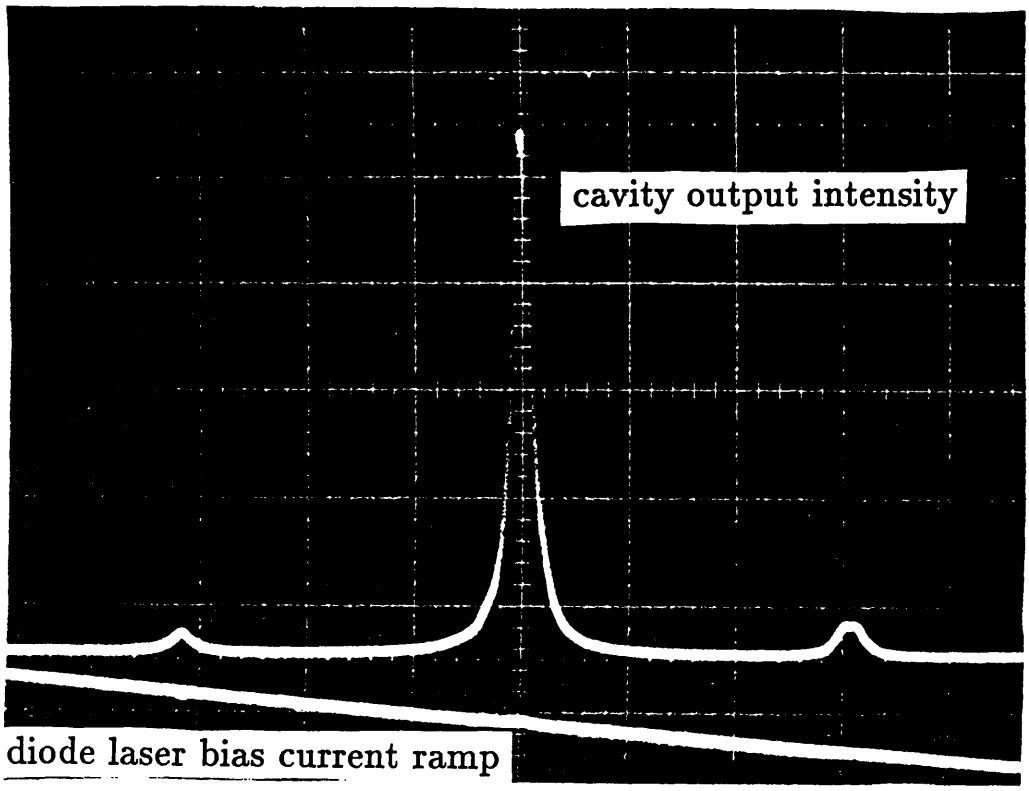

Figure 9. Cavity transmission as a function of frequency detuning from cavity resonance.

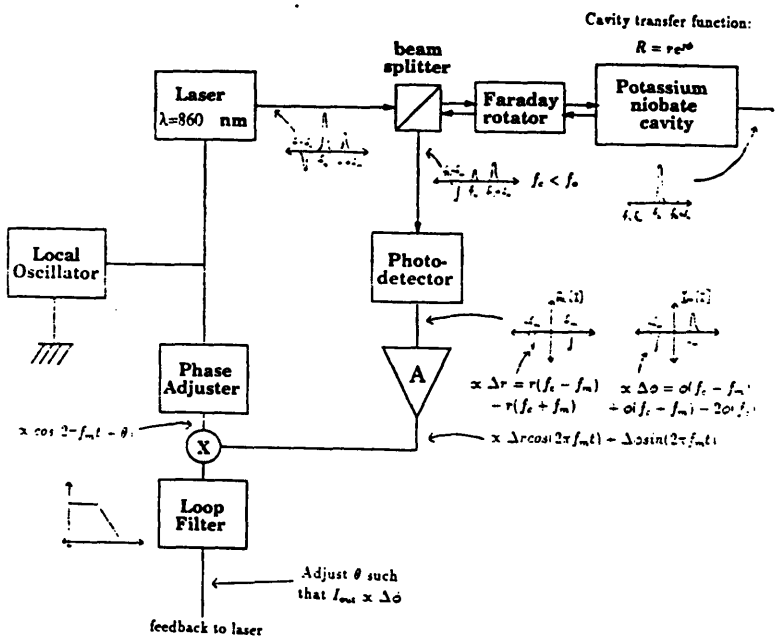

Figure 10. Pound-Drever locking scheme.

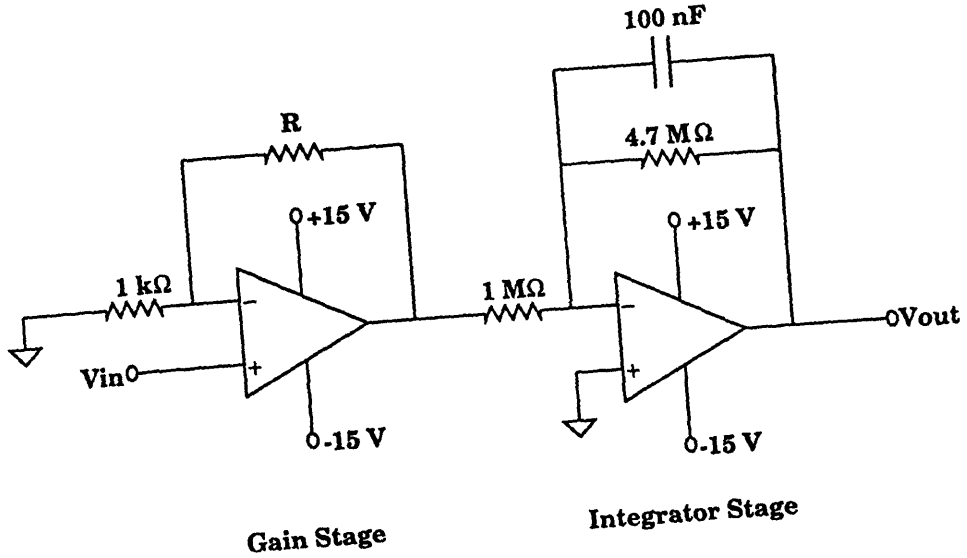

Figure 11. Loop filter circuit.

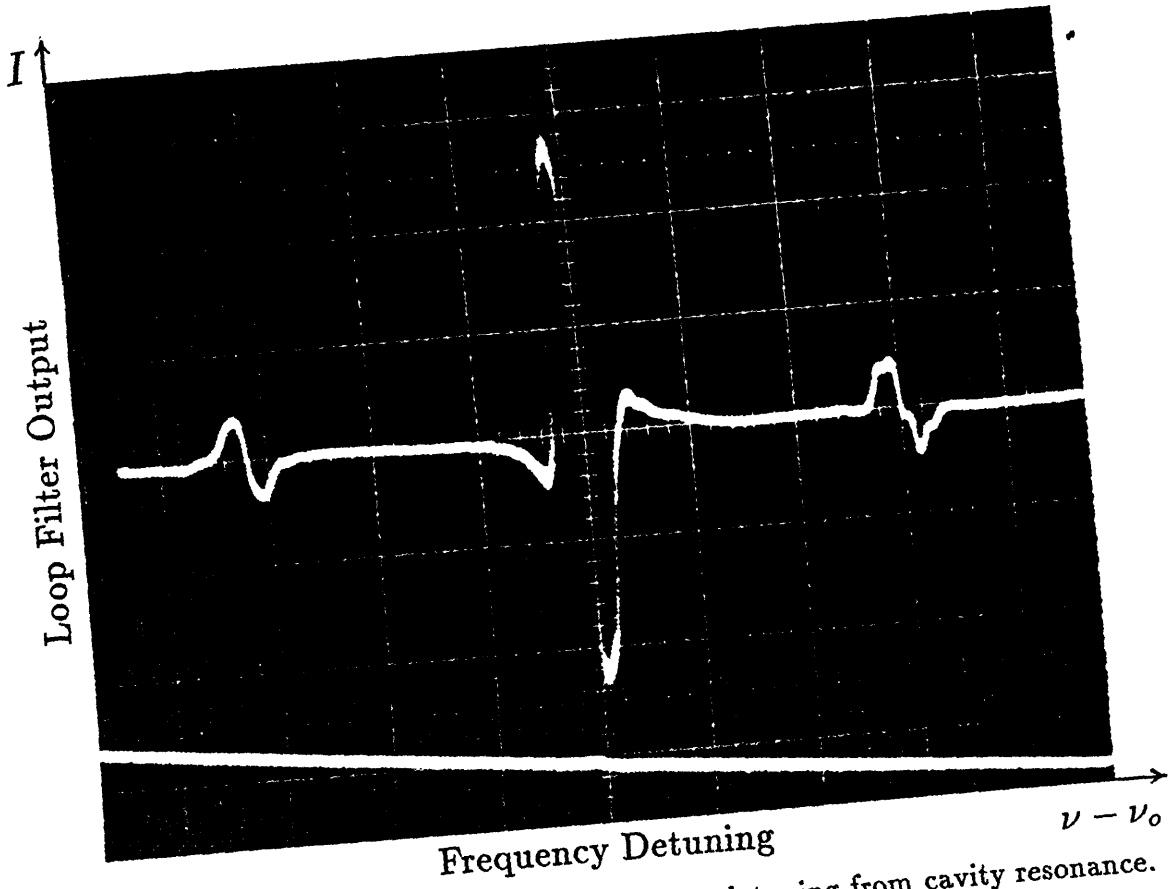

Figure 12. Error signal as a function of frequency detuning from cavity resonance.

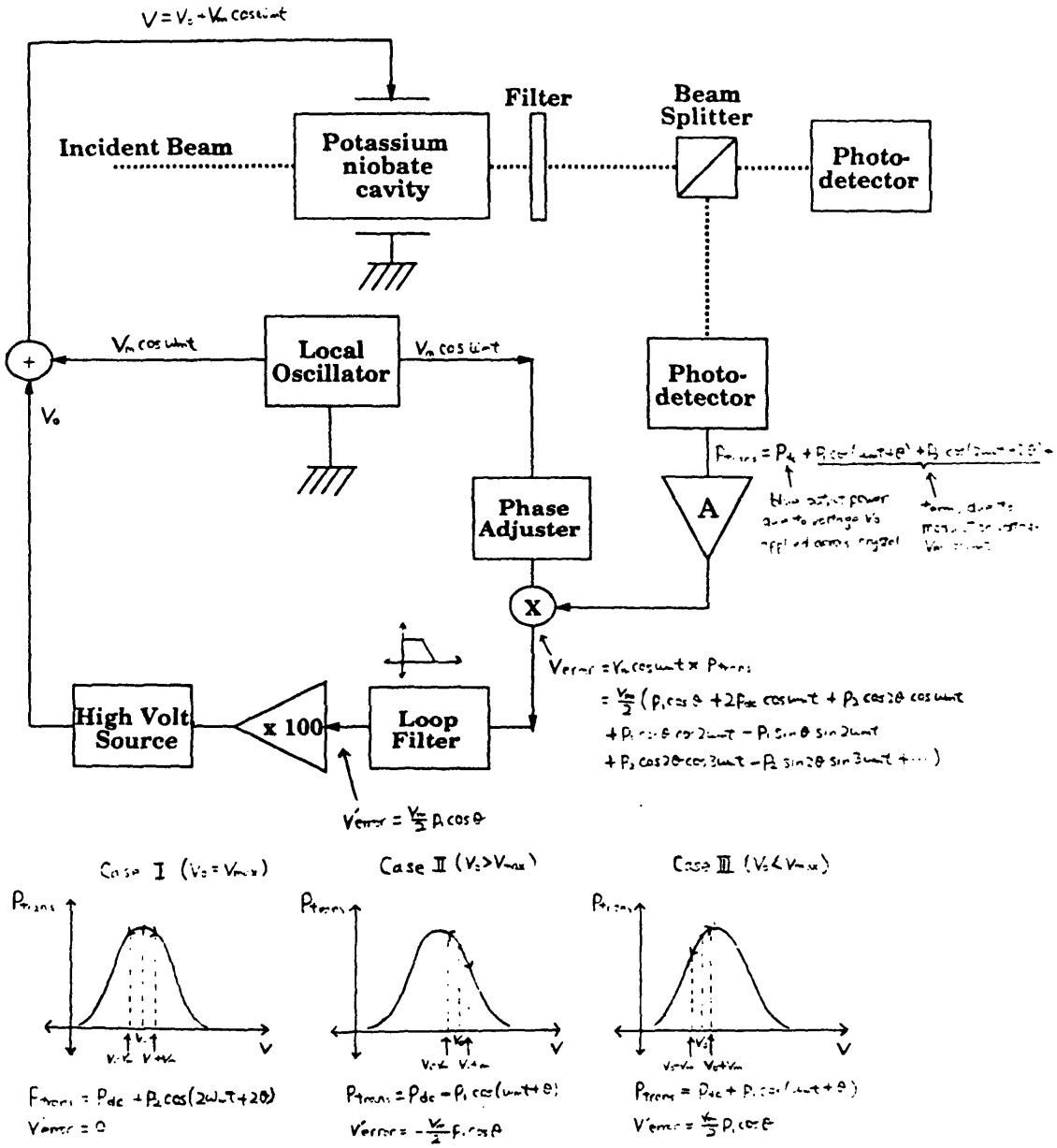

Figure 13. Setup for locking the second harmonic output intensity.

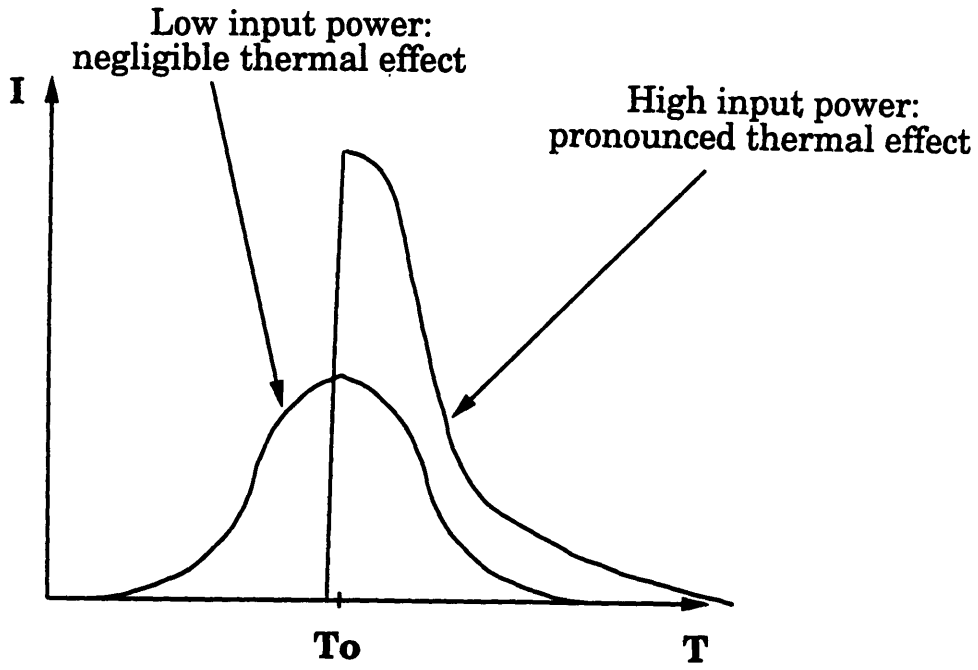

Figure 14. Temperature dependence of second harmonic intensity in the vincinity of phasematching.

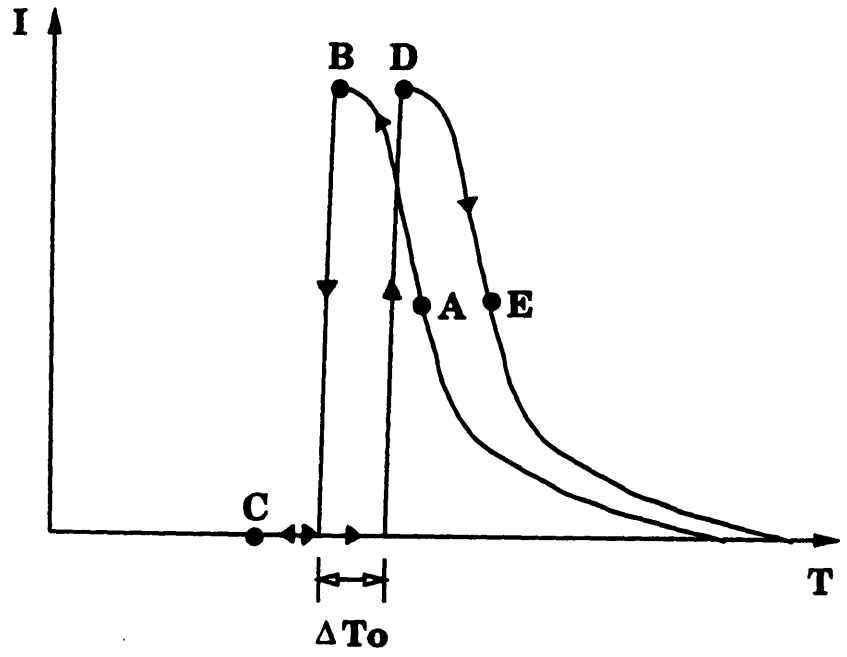

Figure 15. Hysteresis effect of second harmonic intensity as a function of temperature.

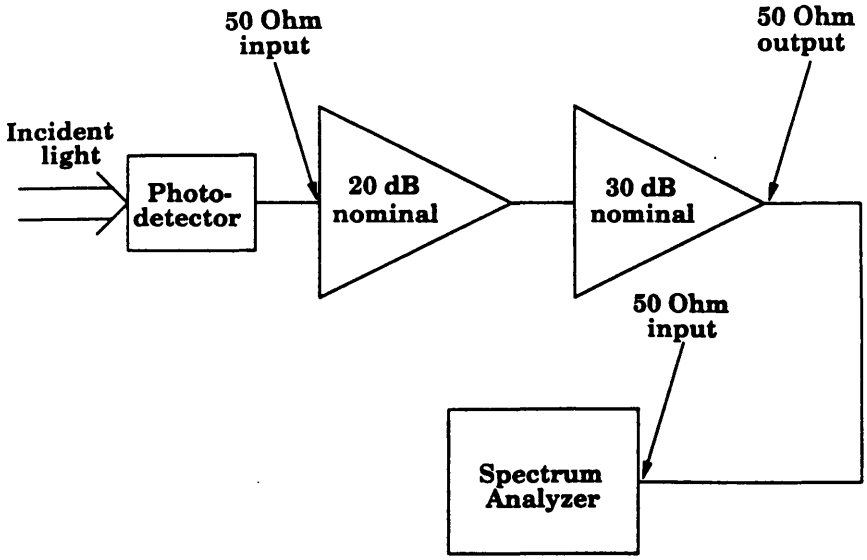

Figure 16. Noise detection scheme.

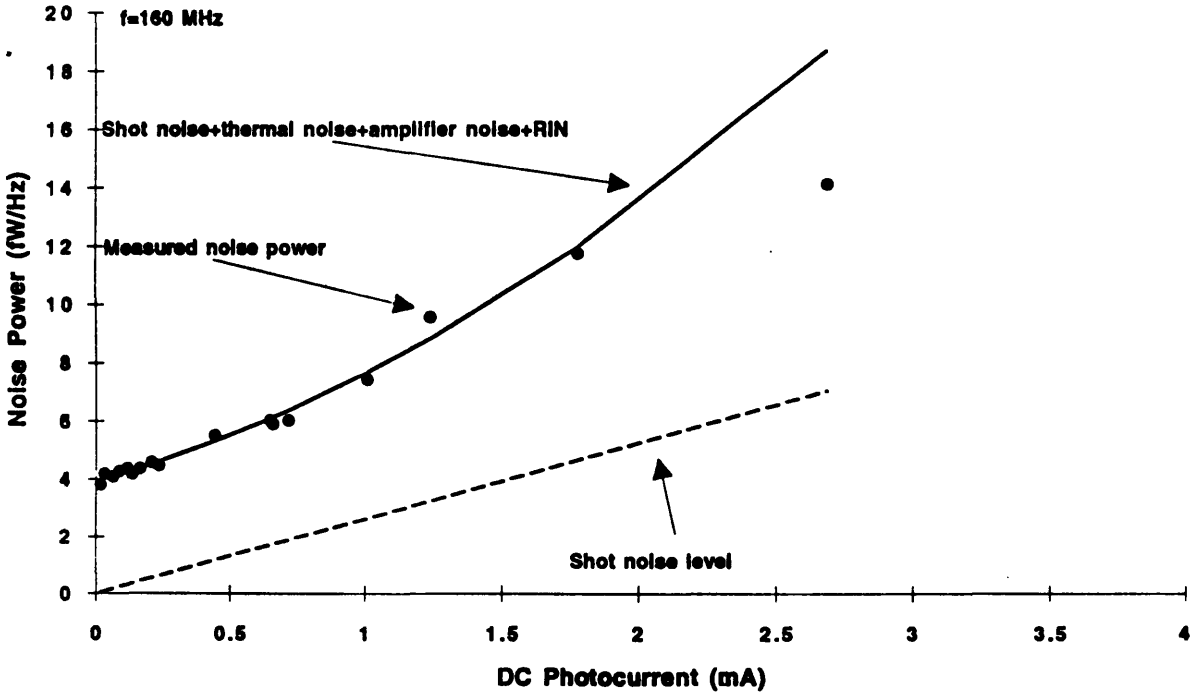

Figure 17. Noise power of laser output field.

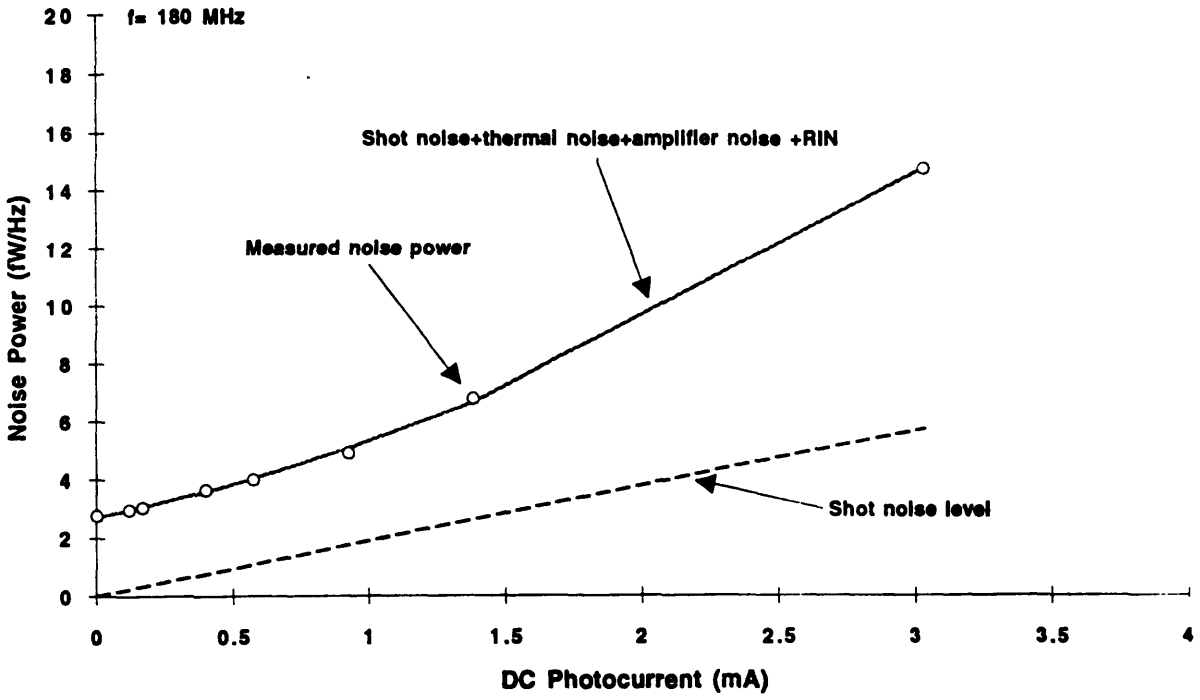

Figure 18. Noise power of laser output field following reflection from a mirror.

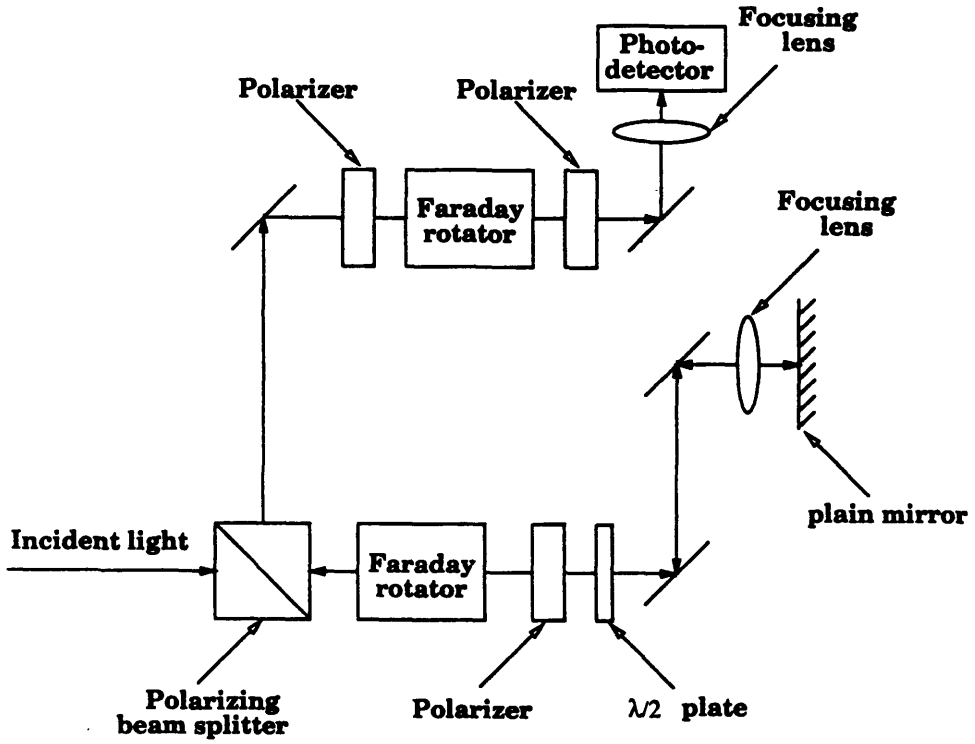

Figure 19. Optical path of laser beam reflected from a plain mirror.

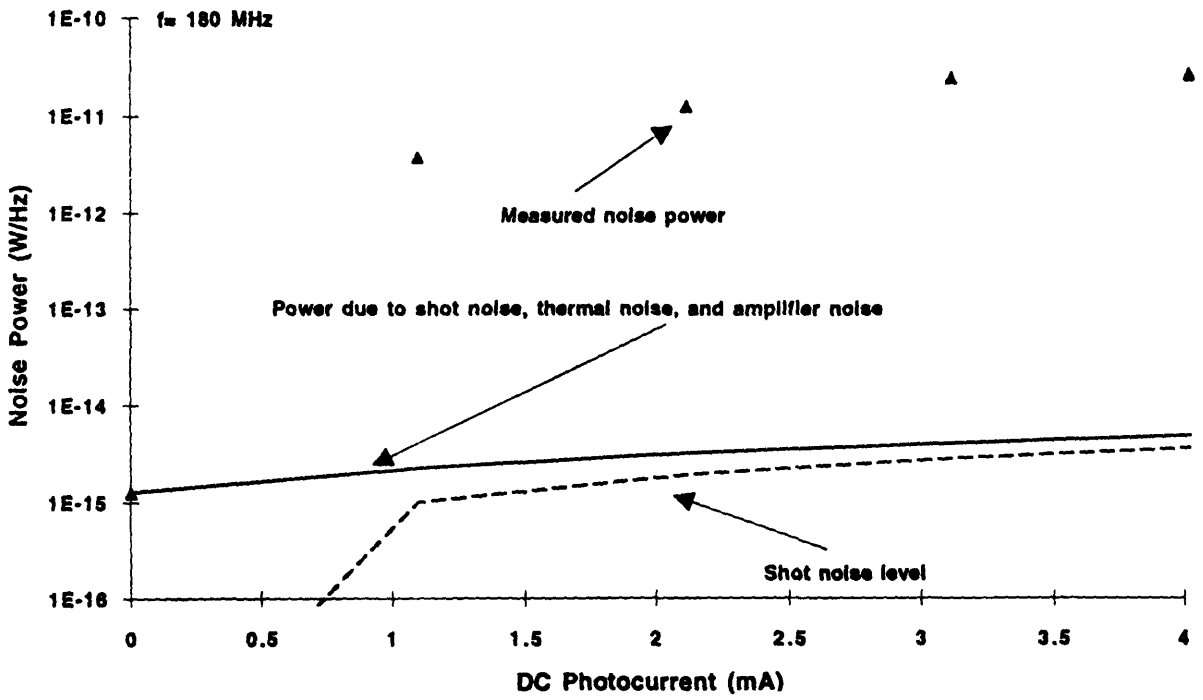

Figure 20. Noise power of reflected fundamental field.

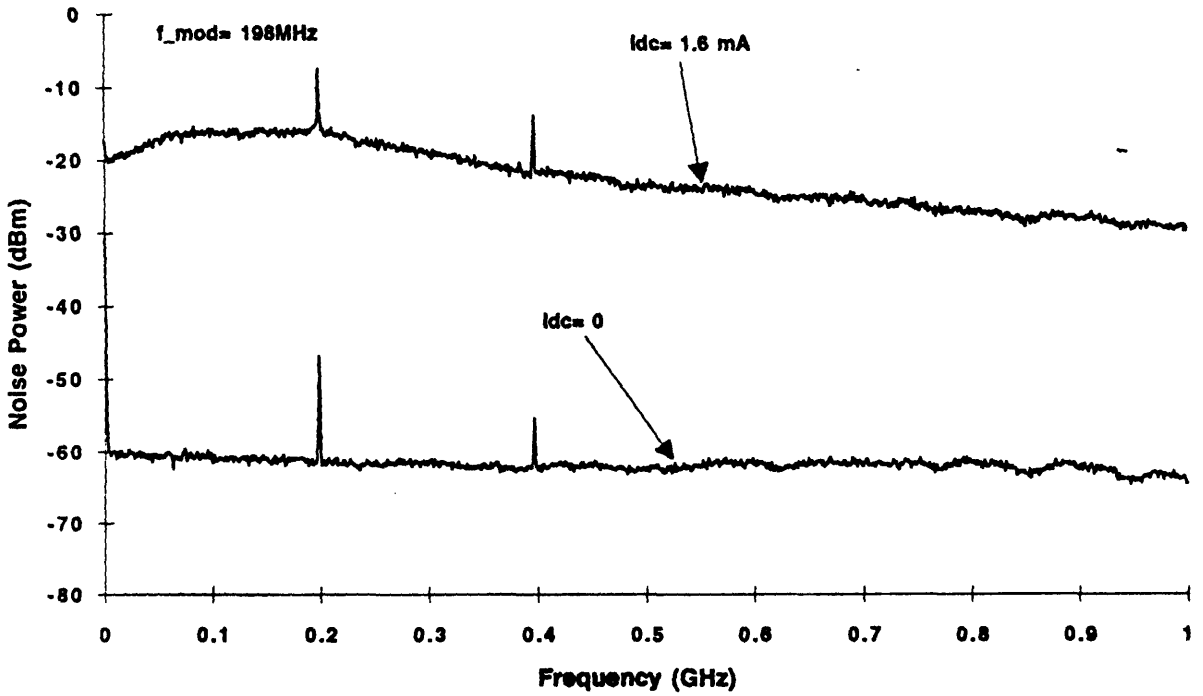

Figure 21. Measured noise spectrum of reflected fundamental field. The detected photocurrent is 1.6 mA (upper trace). The lower trace shows the noise spectrum with the laser beam blocked from the photodetector.

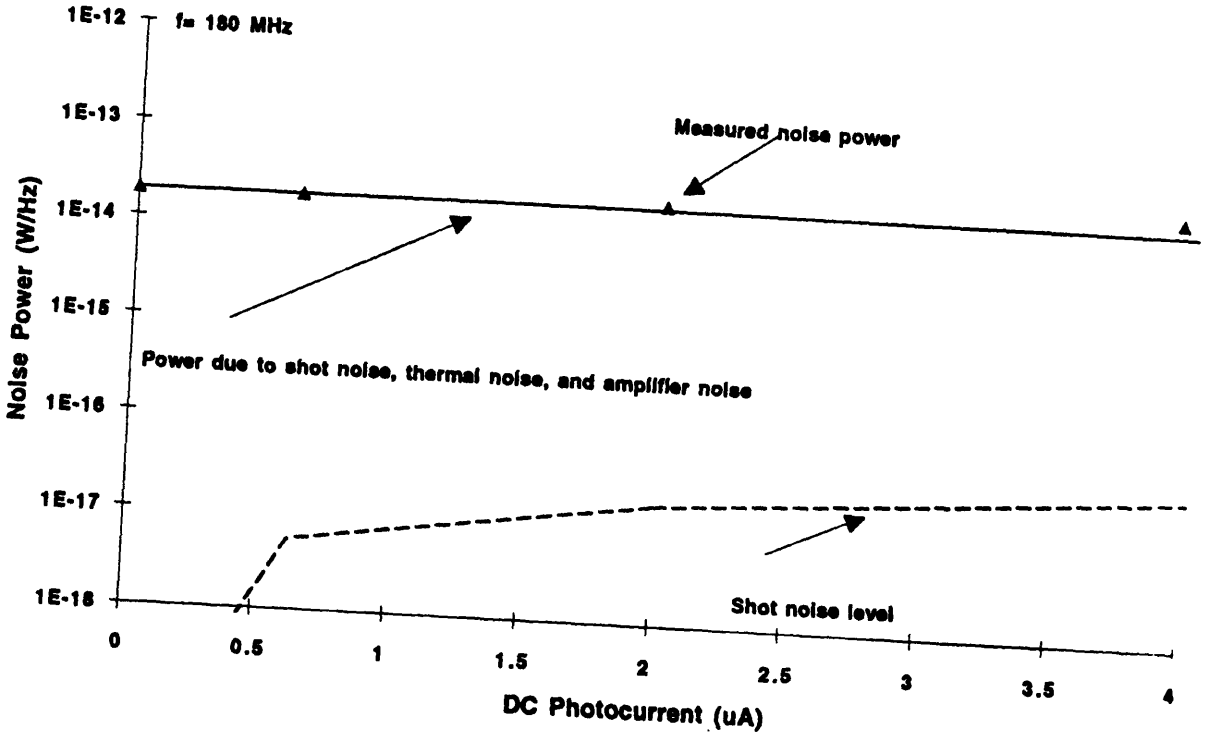

Figure 22. Noise power of transmitted second harmonic field.

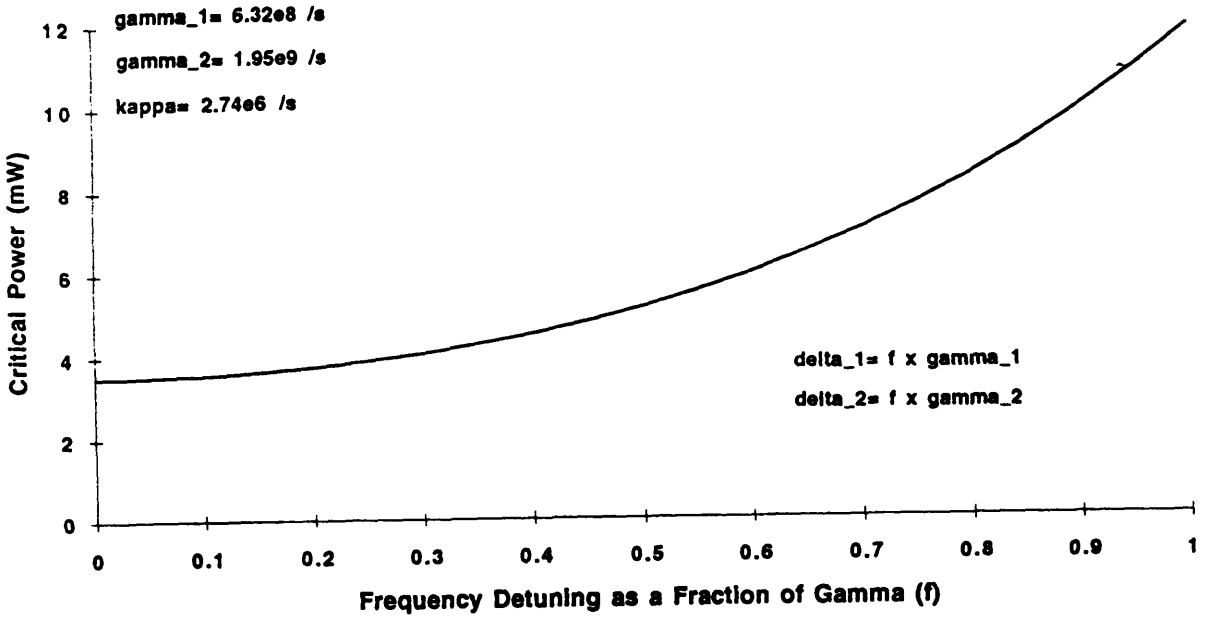

Figure 23a. Critical power as a function of frequency detuning.

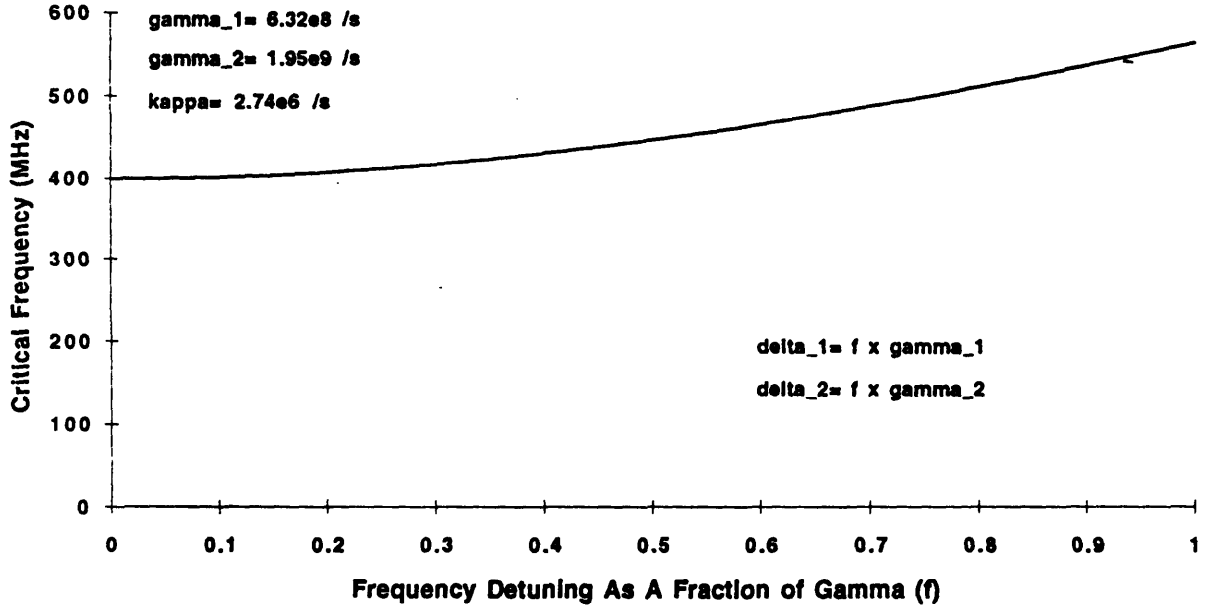

Figure 23b. Critical oscillation frequency as a function of frequency detuning.

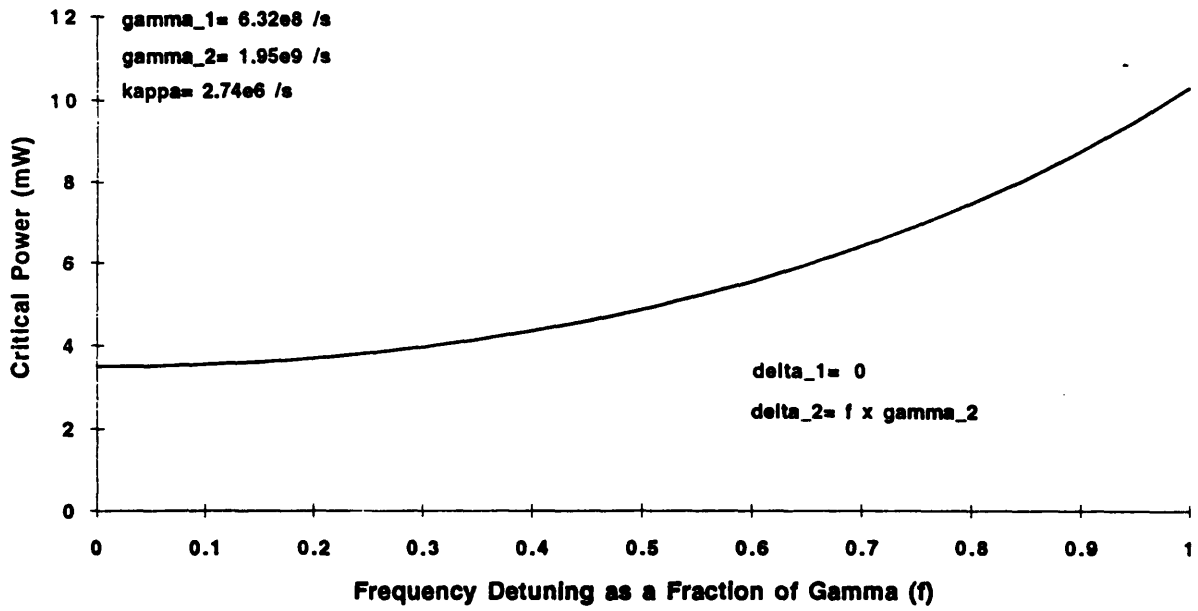

Figure 24a. Critical power as a function of frequency detuning in the second harmonic mode only.

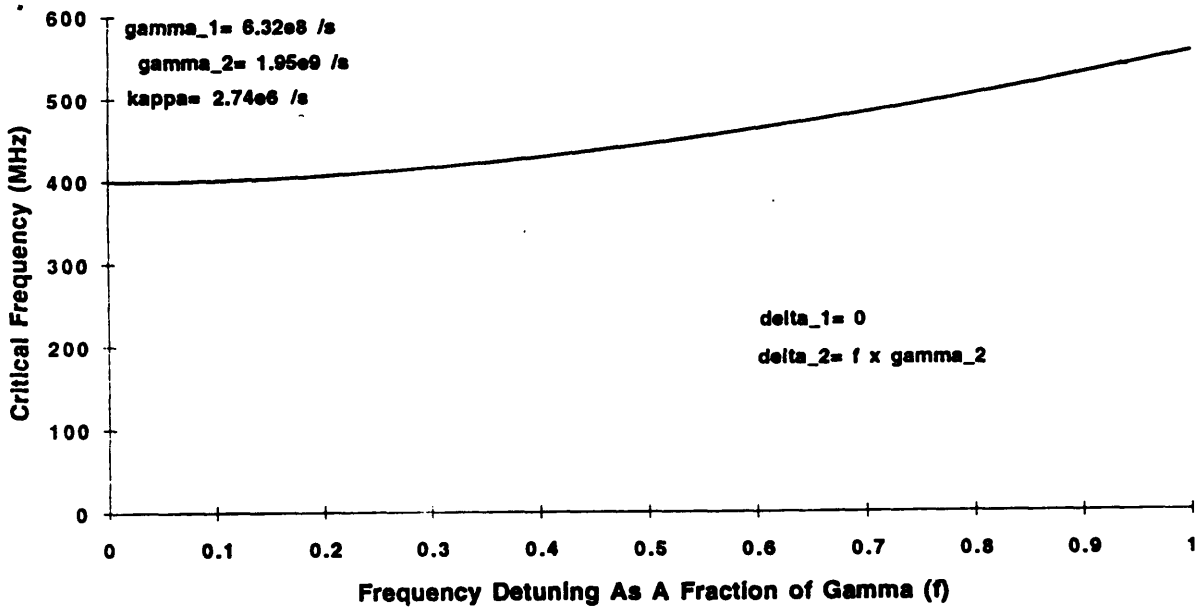

Figure 24b. Critical oscillation frequency as a function of frequency detuning in the second harmonic mode only.

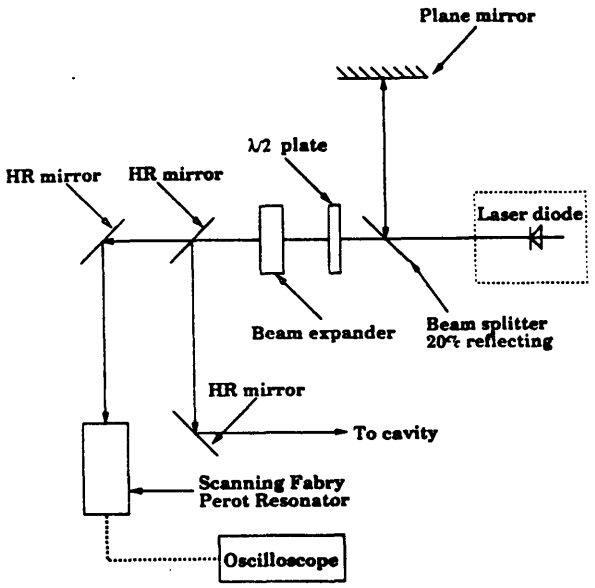

Figure 25a. Laser linewidth reduction scheme. Optical feedback is provided by plain mirror.

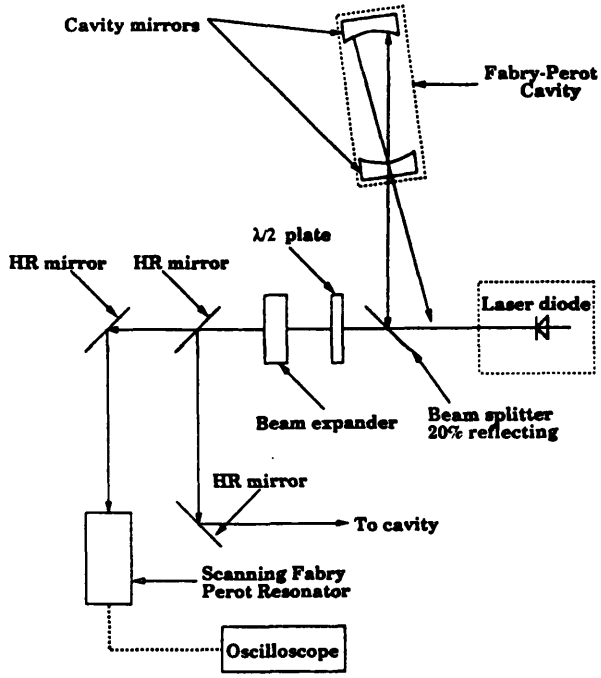

Figure 25b. Laser linewidth reduction scheme. Optical feedback is provided by Fabry-Perot resonator.

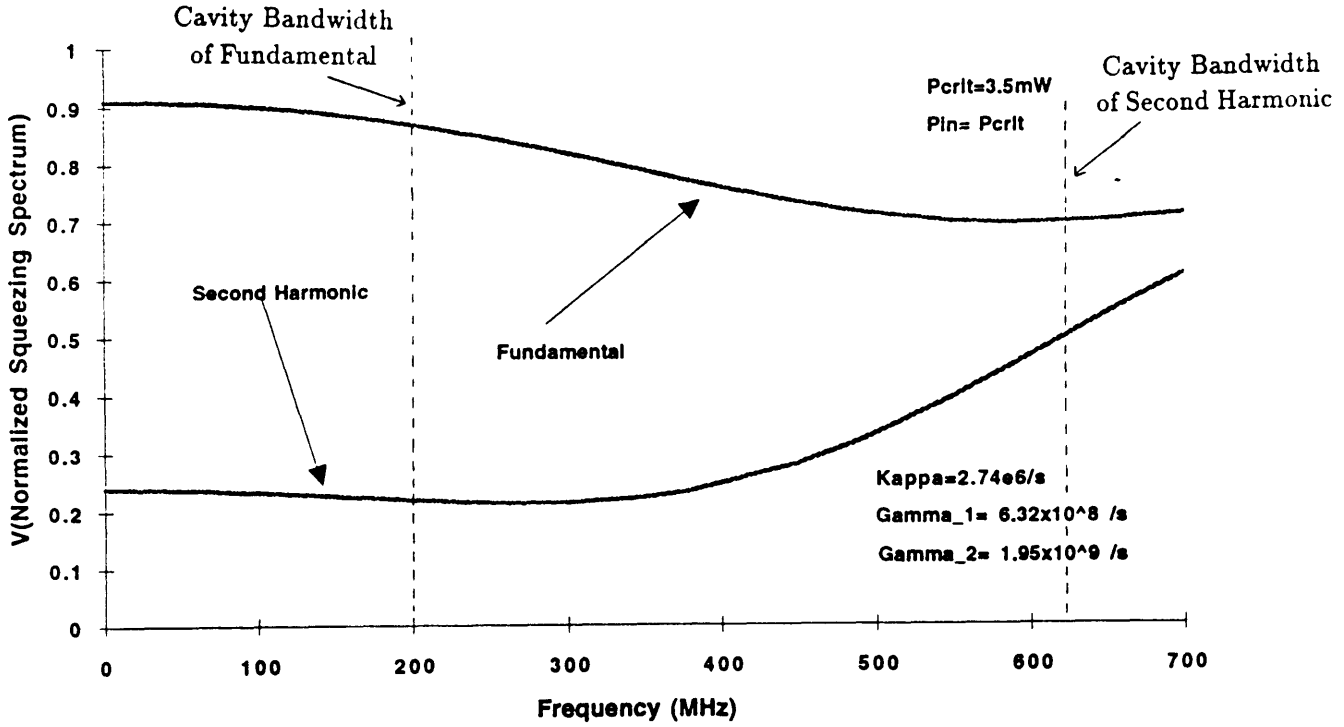

Figure 26a. Squeezing spectrum for $P_{in} = P_{crit}$.

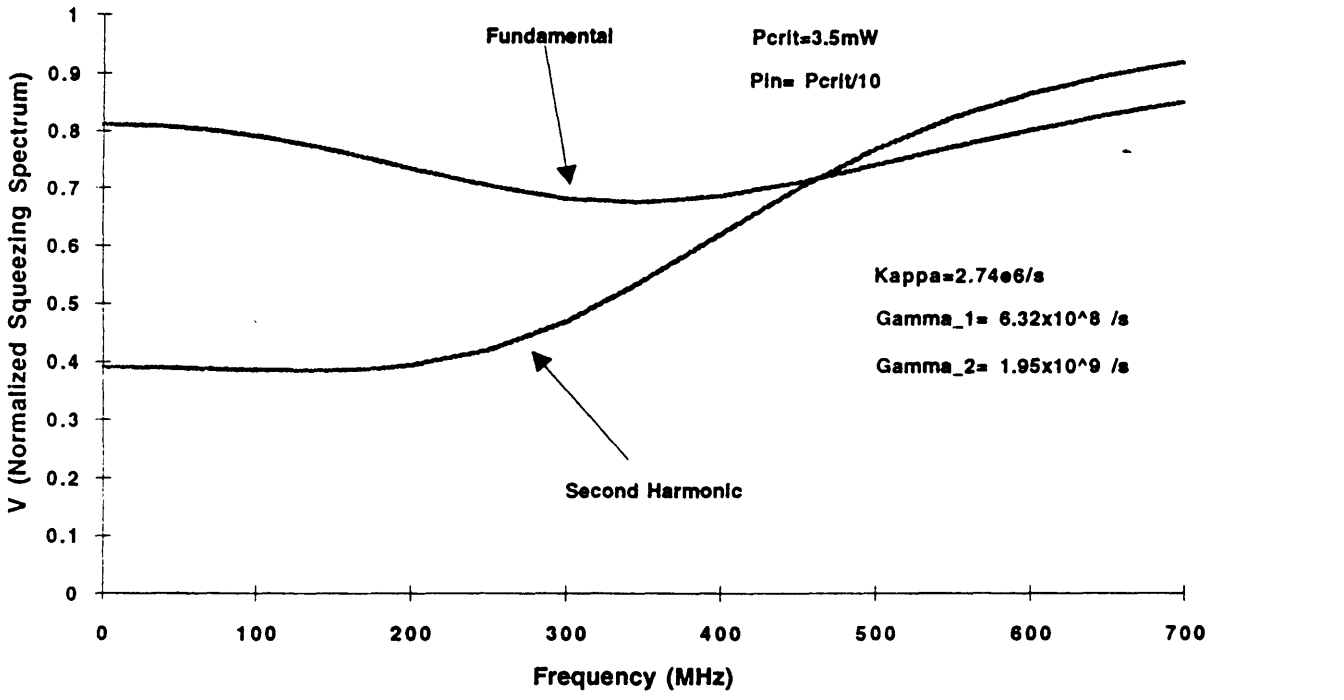

Figure 26b. Squeezing spectrum for $P_{in} = \frac{1}{10} P_{crit}$.

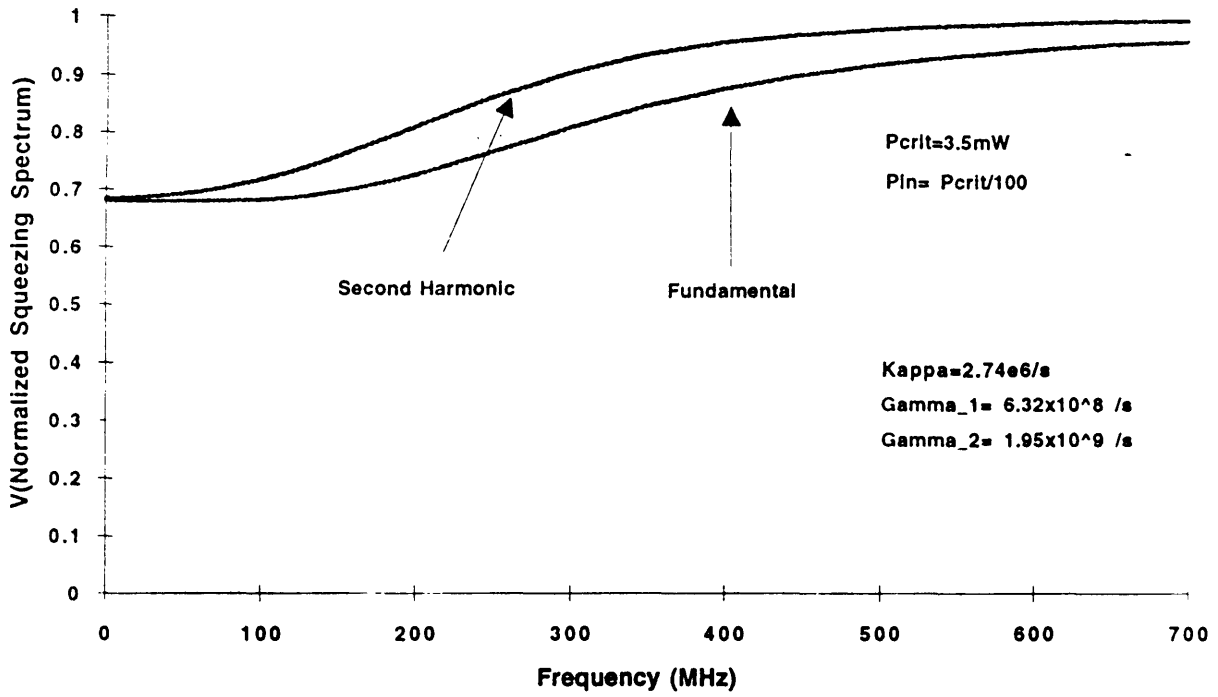

Figure 26c. Squeezing spectrum for $P_{in} = \frac{1}{100} P_{crit}$.

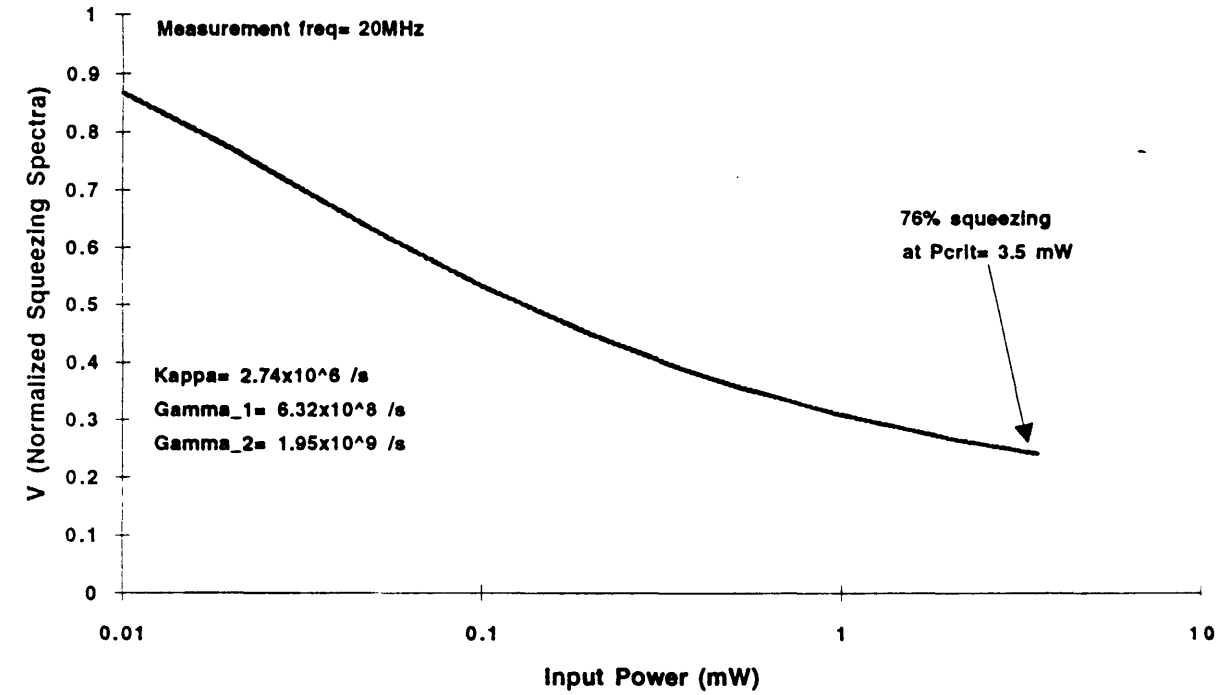

Figure 27a. Power dependence of squeezing in the second harmonic mode at 20MHz.

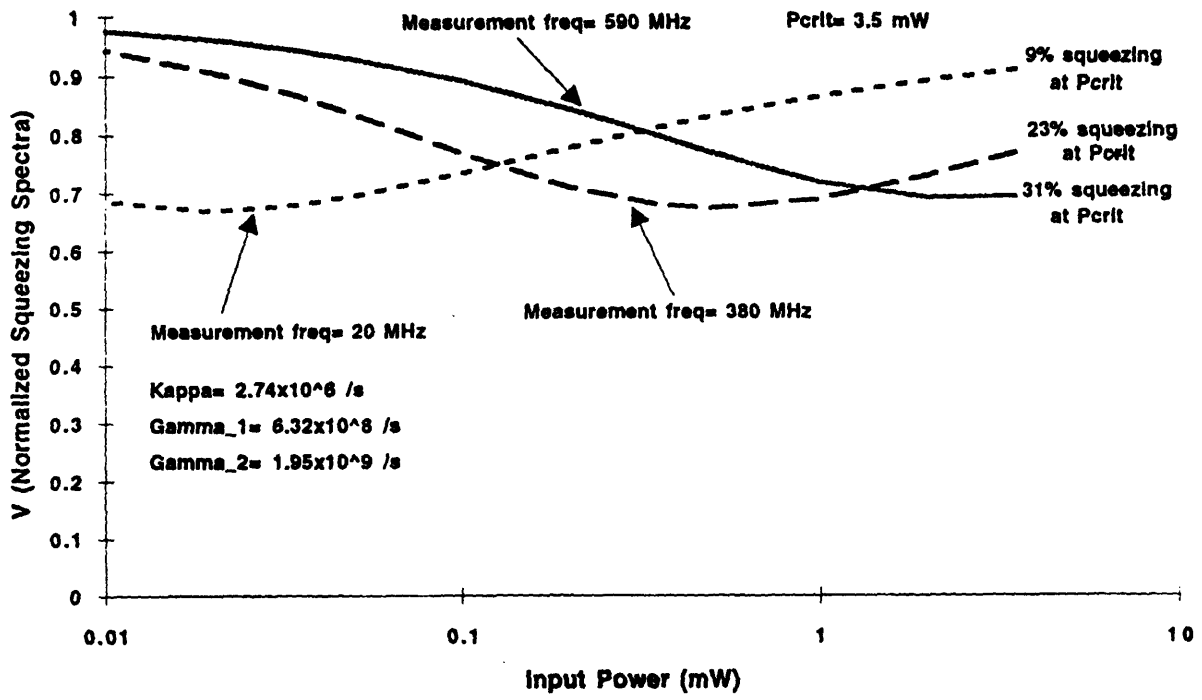

Figure 27b. Power dependence of squeezing in the fundamental mode at 20MHz, 380MHz, and 590MHz.

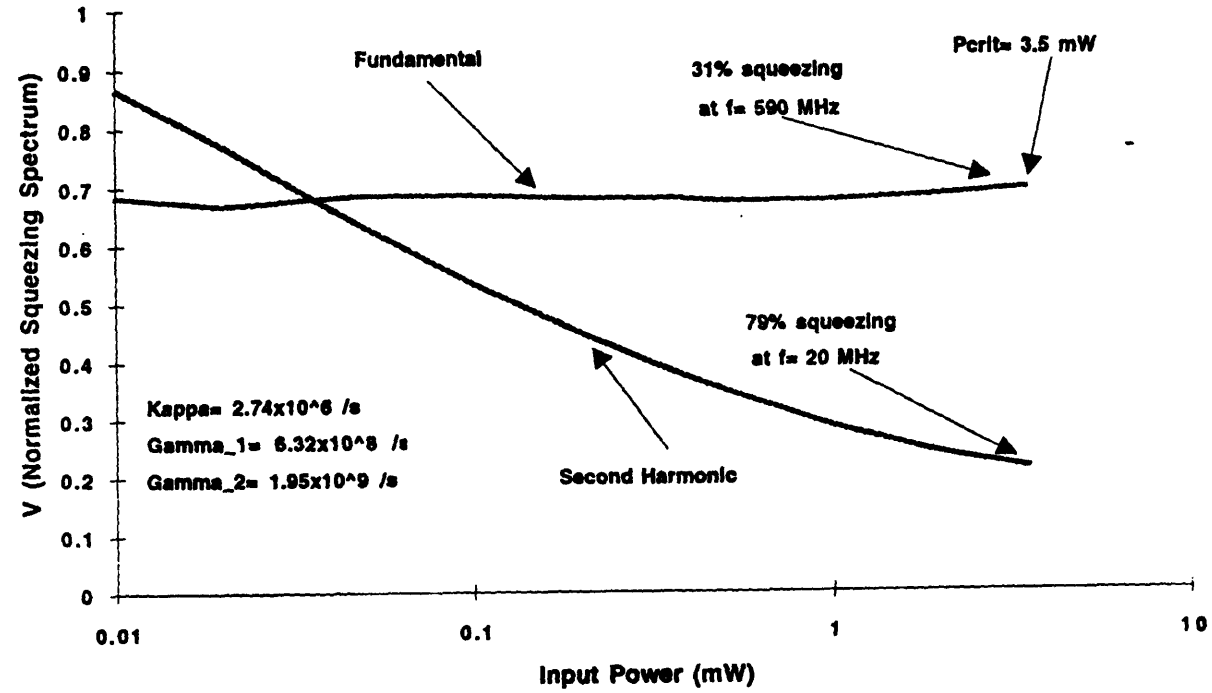

Figure 27c. Power dependence of the maximum achievable squeezing in the fundamental and second harmonic modes.

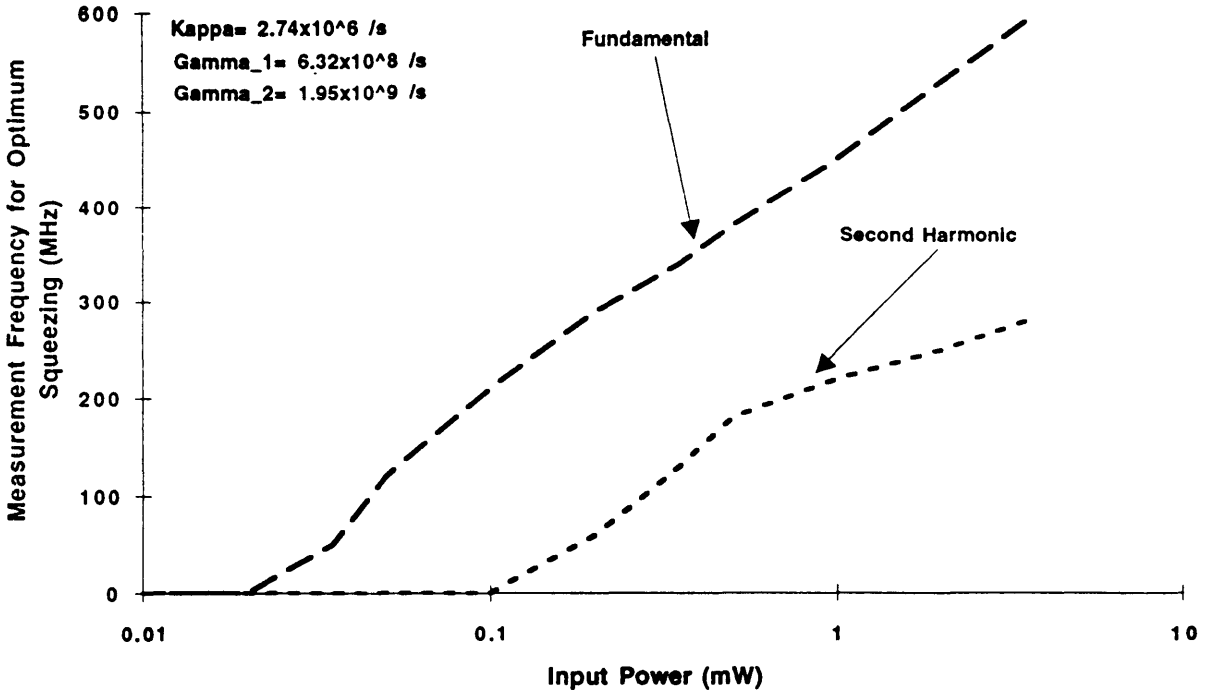

Figure 28. Optimum measurement frequency for squeezing as a function of input power.